Journal of Medicinal Chemistry

Article

Structure-based Drug Design of Potent Pyrazole Derivatives against Rhinovirus Replication

Laurene Da Costa, Els Scheers, Antonio Coluccia, Adriano Casulli, Manon Roche, Carole Di Giorgio, Johan Neyts, Thierry Terme, Roberto Cirilli, Giuseppe La Regina, Romano Silvestri, Carmen Mirabelli, and Patrice Vanelle

J. Med. Chem., **Just Accepted Manuscript** • Publication Date (Web): 28 Aug 2018

ACS Publications

is published by the American Chemical Society. 1155 Sixteenth Street N.W., Washington, DC 20036

Structure-based Drug Design of Potent Pyrazole Derivatives against Rhinovirus Replication

Laurène Da Costa,[†,#] Els Scheers,[‡,#] Antonio Coluccia,[§] Adriano Casulli,[∞] Manon Roche,[†] Carole Di Giorgio,[⊥] Johan Neyts,[‡] Thierry Terme,[†] Roberto Cirilli,[∥] Giuseppe La Regina,[§] Romano Silvestri,[§] Carmen Mirabelli,[‡] Patrice Vanelle[†,]*

[†] Aix-Marseille Univ, Institut de Chimie Radicalaire, Laboratoire de Pharmacochimie Radicalaire, UMR 7273 CNRS, 27 Boulevard Jean Moulin, 13385 Marseille Cedex 05, France

[‡] KU Leuven-University of Leuven, Department of Microbiology and Immunology, Rega Institute for Medical Research, Laboratory of Virology and Chemotherapy, B-3000 Leuven, Belgium

[§] Department of Drug Chemistry and Technologies, Sapienza University of Rome, Laboratory affiliated to Istituto Pasteur Italia-Fondazione Cenci Bolognetti, Piazzale Aldo Moro 5, I-00185 Roma, Italy

[∞] WHO Collaborating Centre for the Epidemiology, Detection and Control of Cystic and Alveolar Echinococcosis. European Reference Laboratory for Parasites. Department of Infectious Diseases, Istituto Superiore di Sanità, Viale Regina Elena 299, I-00161, Rome, Italy

[∥] Centro nazionale per il controllo e la valutazione dei farmaci, Istituto Superiore di Sanità, Viale Regina Elena 299, I-00161 Roma, Italy

[L] Aix-Marseille Univ, CNRS, IRD, Avignon Université, IMBE UMR 7263, Laboratoire de Mutagénèse Environnementale, 27 Boulevard Jean Moulin, 13385 Marseille Cedex 05, France

KEYWORDS: RV, VP1 protein, capsid binder, chiral inhibitors, heterocycles.

ABSTRACT: Rhinoviruses (RVs) have been linked to exacerbations of many pulmonary diseases, thus increasing morbidity and/or mortality in subjects at risk. Unfortunately, the wide variety of RV genotypes constitutes a major hindrance for the development of Rhinovirus replication inhibitors. In the current investigation, we have developed a novel series of pyrazole derivatives that potently inhibits the Rhinovirus replication. Compounds **10e** and **10h** behave as early-stage inhibitors of Rhinovirus infection with a broad-spectrum activity against RV-A and RV-B species (EC_{50} < 0.1 μM). We also evaluate the dynamics of the emerging resistance of these promising compounds and their *in vitro* genotoxicity. Molecular docking experiments shed light on the pharmacophoric elements interacting with residues of the drug-binding pocket.

INTRODUCTION

Rhinoviruses (RVs) are among the most common viruses worldwide. With a respiratory tract tropism, these infectious agents of the *Picornaviridae* family (genus *Enterovirus*) are the major causative agents of upper respiratory tract infections.[1,2] Besides being the etiological agent of the "common cold", they are also associated with acute otitis media (AOM) development in pediatric populations,[3,4,5] and sinusitis.[6,7] For the past decade, RVs have been identified as the cause of exacerbations of chronic pulmonary diseases in infants, the elderly, and immunocompromised patients.[8,9] RVs have a strong impact on asthma-related morbidity and mortality in these populations.[10,11,12,13] RV infections have also been reported to lead to worsening of chronic obstructive pulmonary disease (COPD),[14,15] and cystic fibrosis.[16,17]

Currently, more than three hundred million people suffer from chronic pulmonary illnesses. Industrial and academic laboratories are therefore reviving research on RVs, seeking to provide new therapeutic options.

As commonly observed in the Picornavirales order, RVs are composed of a positive-sense single-stranded RNA surrounded by a protein shell called capsid. To date, 167 types of RVs have been identified by molecular-based phylogenetics and classified in three species, namely RV-A, RV-B, and RV-C.[18,19] Following entry, viral RNA is translated into a single polyprotein, which is further processed into four structural and seven non-structural proteins required for the replication. The structural proteins (VP1-VP4) form the characteristic icosahedral capsid of all members of the genus *Enterovirus*.[20] The assembly of these four viral proteins has specific structural features enabling it to serve as a cellular binding site: a star-shaped dome on the icosahedral 5-fold axis from five VP1 units and a depression surrounding the dome that forms a "canyon".[21,22,23] The majority of RV-A and RV-B binds to ICAM-1, one of the members of the immunoglobulin superfamily, through the "canyon"[24] but the pentameric dome of the minor group (10% of all RV-A and RV-B) has an affinity for the low-density lipoprotein receptor (LDL-R).[25] Furthermore, it was recently reported that RV-C15 uses cadherin-related family member 3 (CDHR3) as its cellular receptor.[26,27] Viruses of the *Enterovirus* genus, and in particular RV-A and RV-B, are characterized by the presence of a hydrophobic cavity under the floor of the canyon. In many RVs, this cavity contains a small lipid molecule of cellular origin, called "pocket factor".[28] This molecule stabilizes the viral capsid and takes part in the capsid uncoating process during viral entry.

The high genetic and antigenic variability across RVs hampers the development of vaccines, prompting the development of antiviral compounds instead. To do so, conserved proteins like the

viral protease 3C (rupintrivir),[29,30] and a conserved process like viral entry (capsid binders) were identified as antiviral targets. More specific, capsid binders target the hydrophobic pocket and block virus uncoating and/or attachment.[31,32,33,34,35] Despite forty years of extensive antiviral research, no antiviral drug has been approved yet for the treatment of rhinovirus infections. The best-studied and now reference capsid binder is pleconaril (WIN 63843, **1**),[36] developed by Schering-Plough. However, its clinical development for the treatment of RV infections was halted due to poor *in vivo* activity and rapid selection of drug-resistant variants. Two capsid binders are now in the advanced phase of development: vapendavir (BTA-798, **2**) (Aviragen Therapeutics®, clinical trials phase IIb, NCT01175226) (Figure 1A) and AZN001 (AstraZeneca, pre-clinical trials),[37] proving that research on this class of inhibitors is actively pursued.

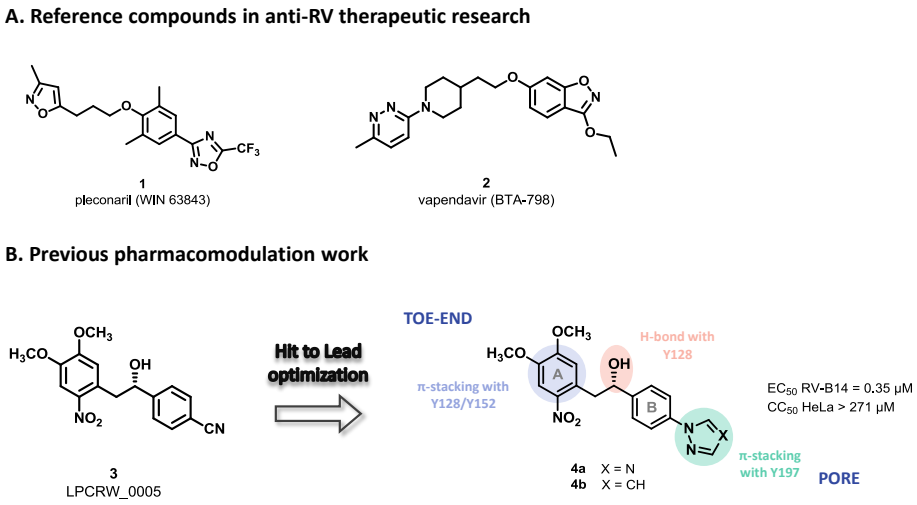

Figure 1. A. Structure of known capsid binders **1** and **2** of RVs; B. "Pore" side pharmacomodulations: antiviral activity against RV-B14 and key ligand/protein interactions.

Since 2014, we have been developing a new chiral scaffold with a promising antirhinoviral profile against RV-B. The hit compound **3** (**LPCRW_0005**) revealed the same antiviral profile and the same binding pocket as pleconaril **1**.[38,39] Extensive pharmacomodulations were required

to extend the scaffold to fill the "pore" side within this hydrophobic pocket.[40] Thus, we discovered new hits, compounds **4**, substituted with pyrazole or triazole moieties, with a potent antiviral activity against RV-B14 (Figure 1B).[41]

Here, we carried out a new heterocyclic pharmacomodulations aimed to lengthen our scaffold. At the "pore" side, we evaluated the 4-pyridinyl, 1*H*-pyrazol-1-yl, or 1*H*-triazol-1-yl analogues. Whereas at the "toe-end" side, we studied the introduction of heteroaromatic 5-member rings and halogen atoms. The latter were placed at position 4 of ring A as suggested by docking studies and, in addition, they kept the same interatomic distances as **1**. This led us to identify two analogues with an efficacy in the nanomolar range. Both their broad-spectrum activity (RV-A and RV-B) and their antiviral mechanism of action were explored. Moreover, due to the presence of a nitro group on cycle A, we evaluated their *in vitro* genotoxicity using a micronucleus test. In addition, *in vitro* emerging resistance against RV-B14 was assessed and compared with **1**. Evaluations of the new structure-activity relationships (SARs) were also performed based on *in silico* molecular docking.

RESULTS

Synthesis of the heterocyclic antirhinoviral library.

The synthetic routes for all derivatives are described in Scheme 1. The 2-nitrobenzyl chlorides **6a-6d** were prepared by reduction of carboxylic acids **5a-5d** with a stabilized BH_3.THF solution, and subsequent chlorination with $SOCl_2$.

The hetero-functionalization on the "pore" side was carried out using an organic electron donor, tetrakis(dimethylamino)ethylene (TDAE). This agent generates a carbanion from benzyl chloride by two sequential single-electron transfer (SET).[42] A nucleophilic addition on the C=O bond of aldehyde derivatives then yields to form the chiral secondary alcohol linker (Scheme 1,

route c). Thus, pyrazole and triazole derivatives **9c-9f** were obtained from commercial reagents (4-(1*H*-pyrazol-1-yl)benzaldehyde and 4-(1*H*-1,2,4-triazol-1-yl)benzaldehyde) and **6a-6c**. For pyridinic analogues, we prepared upstream the aldehyde **8** from a Suzuki-Miyaura cross-coupling reaction (Scheme 1, route d) and a TDAE strategy led us to compounds **9a** and **9b**.

Finally, the brominated compounds **9b**, **9c** and **9f** underwent in a final pallado-catalyzed coupling to functionalize the "toe-end" position (Scheme 1, route e). $Pd(PPh_3)_2Cl_2$ was used as catalyst to prepare the pyridinic analogues **10a-10c** with yields between 66 and 78%. The last compounds bearing a pyrazole or a triazole nucleus (**10d-10j**) were prepared with the highly reactive catalyst $Pd(dppf)Cl_2$, providing up to 96% yields.

Scheme 1. General procedure for the synthesis of the heterocyclic antirhinoviral library[a]

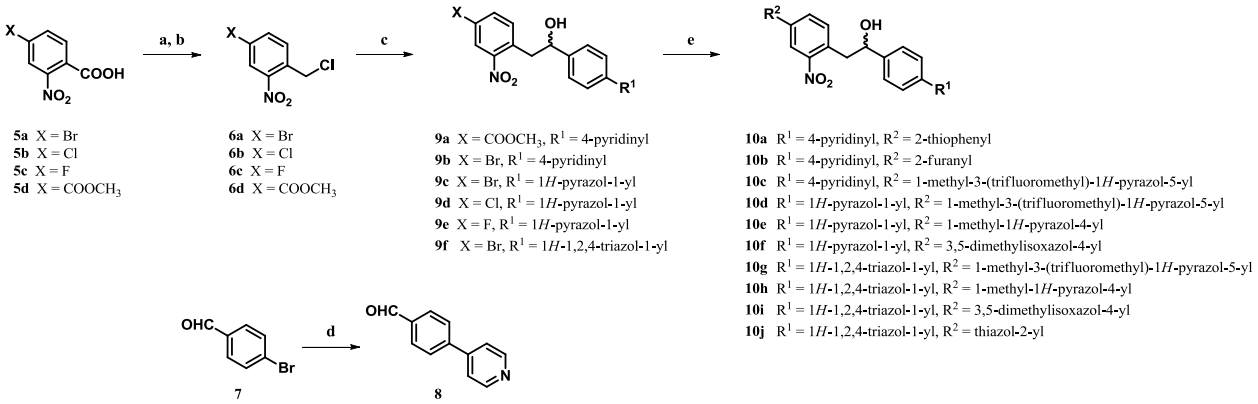

[a] Reagents and conditions: (a) BH_3-THF, THF, rt, 3 days; (b) $SOCl_2$, Et_3N, CH_2Cl_2, rt, 12 h, 79-92% (2 steps); (c) **8**, 4-(1*H*-pyrazol-1-yl)benzaldehyde or 4-(1*H*-1,2,4-triazol-1-yl)benzaldehyde, TDAE, DMF, 1) -20 °C, 1 h, 2) rt, 12 h, 13-35%; (d) pyridin-4-ylboronic acid, $Pd(PPh_3)_4$, K_2CO_3, DMF/Water, MW (130 °C), 30 min, 85%; (e) boronic acid derivative, $Pd(PPh_3)_2Cl_2$, K_2CO_3, dioxane, 80 °C, 12 h, 66-78% for **10a-10c** or boronic acid derivative, $Pd(dppf)Cl_2$, K_2CO_3, dioxane/water, 80 °C, 12 h, 54-96% for **10d-10j**.

Identification of antirhinoviral compounds *via* CPE reduction assays

The newly-synthesized compounds were evaluated for *in vitro* antiviral activity against RV-B14 in a cell-based CPE reduction assay on HeLa Rh cells. Antiviral activity is expressed as the concentration at which 50% of virus-induced CPE was inhibited (EC_{50}). Compound cytotoxicity (CC_{50}) was assessed in parallel in compound-treated, uninfected cells. Pleconaril **1** was used as a reference capsid binder. Compounds were classified according to the moieties inserted on the "pore" side: 4-pyridinyl, 1*H*-pyrazol-1-yl, or 1*H*-triazol-1-yl. From there, the antirhinoviral properties of (aza)-heterocycles as well as halogens (chlorine, bromine, and fluorine) were studied.

We first assessed the antiviral activity of the pyridinic analogues **9a**, **9b**, and **10a-10c** but we could not detect an improvement in EC_{50} compared to the hits **4** (Table 1). In contrast, 6 out of 11 compounds bearing a pyrazole or a triazole nucleus (**9c-9f** and **10d-10j**) on the "pore" side were more potent against RV-B14 than **4**, especially those substituted with a 1-methyl-1*H*-pyrazol-4-yl group towards the "toe-end" side (**10e** and **10h**), with EC_{50} values of 0.2 μM and SI > 1235. Substitution of a trifluoromethyl group on the pyrazole moiety (**10d** and **10g**) slightly increased the EC_{50} values of the compounds and significantly affected the cytotoxicity of the respective compounds (CC_{50} = 14-21 μM), thereby decreasing their selectivity index. The dimethylisoxazol moieties (**10f** and **10i**) induced a complete loss of antiviral activity against RV-B14. These observations underline the significance of steric hindrance on the "toe-end" side.

Brominated analogues **9c** and **9f** showed a similar antiviral activity but a less desirable SI due to a considerable anti-metabolic activity (CC_{50} < 39 μM). To overcome this toxicity, the efficacy of chlorinated (**9d**) and fluorinated (**9e**) compounds was evaluated. By providing fluorine or

chlorine atom, bioisostere of bromine, the cytotoxic effects on HeLa cells were significantly improved ($CC_{50} > 100$).

Overall, these findings indicate that the introduction of a methylpyrazole or chlorine can improve antiviral activity with negligible effect on cell toxicity, thus improving SI. The two most promising hits **10e** and **10h** displayed characteristics warranting further investigation.

Table 1. *In vitro* biological activity of racemic compounds against RV-B14.[a]

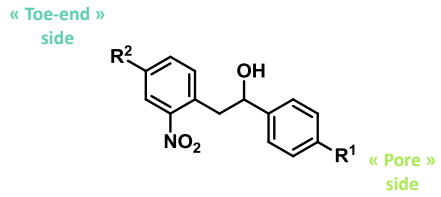

Entry	*(rac)*-Compd	R^1	R^2	EC_{50} RV-B14 (µM)[b]	CC_{50} HeLa (µM)[c]	SI[d]
1	**9a**	4-pyridinyl	$COOCH_3$	6.4 ± 1.1	> 264	> 41
2	**9b**	4-pyridinyl	Br	0.59 ± 0.01	> 250	> 424
3	**10a**	4-pyridinyl		1.3 ± 0.5	> 248	> 191
4	**10b**	4-pyridinyl		1.2 ± 0.2	> 86	> 72
5	**10c**	4-pyridinyl	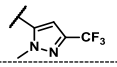	1.0 ± 0.3	> 100	> 100
6	**9c**	1*H*-pyrazol-1-yl	Br	0.25 ± 0.06	22.5 ± 0.7	90
7	**9d**	1*H*-pyrazol-1-yl	Cl	0.128 ± 0.004	> 100	> 781
8	**9e**	1*H*-pyrazol-1-yl	F	8.7 ± 0.1	> 100	> 12
9	**10d**	1*H*-pyrazol-1-yl	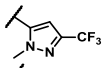	0.5 ± 0.3	14 ± 12	29
10	**10e**	1*H*-pyrazol-1-yl		0.2 ± 0.1	> 247	> 1235
11	**10f**	1*H*-pyrazol-1-yl	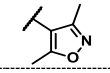	> 247	14 ± 3	-
12	**9f**	1*H*-1,2,4-triazol-1-yl	Br	0.25 ± 0.07	39 ± 1	156
13	**10g**	1*H*-1,2,4-triazol-1-yl	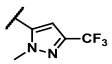	0.4 ± 0.2	21 ± 4	52
14	**10h**	1*H*-1,2,4-triazol-1-yl		0.18 ± 0.05	> 256	> 1422
15	**10i**	1*H*-1,2,4-triazol-1-yl		> 247	> 256	-
16	**10j**	1*H*-1,2,4-triazol-1-yl	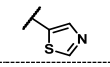	0.4 ± 0.2	44 ± 14	110
17	**1**	pleconaril		0.03 ± 0.02	> 131	> 4039

[a] All values are expressed as median ± Med. Abs. Dev. [b] EC_{50} = 50% effective concentration (concentration at which 50% inhibition of virus-induced cell death is observed). [c] CC_{50} = 50% cytotoxic concentration (concentration at which 50% adverse effect is observed on host cell viability). [d] SI = selectivity index for RV-B14, SI = CC_{50}/EC_{50}. *(rac)* = racemic.

Absolute configuration affects 10e and 10h pharmacological activities.

Having previously observed that chirality significantly influences the activity of this class of compounds,[41] we separated and characterized the enantiomers for compounds **10e** and **10h**. The antiviral activity of the separated enantiomers was then tested against RV-B14 in a cell-based CPE reduction assay.

The enantioseparation was successfully carried out by HPLC on the polysaccharide-based Chiralpak IG-3 chiral stationary phase. The enantiomers collected on a semipreparative scale were submitted to stereochemical characterization according to the multi-step methodology previously described.[41] To determine the absolute configuration of the enantiomers **10h** was used a Mosher's protocol whereas the stereochemistry of **10e** was assigned by a correlative method based on circular dichroism (CD) measurements. This detail methodology is described in the Supporting Information.

Similar to the previous series, we found an increased antiviral activity and selectivity index for the *(S)*-enantiomers (Table 2). The fold increase of EC_{50} of these enantiopure compounds compared to the racemic mixture was more pronounced than that observed in the previous series.[41] Despite *(R)*-**10e** enantiomer retained the antiviral activity, compound *(S)*-**10e** gained 5.7-fold antiviral potency, whereas *(S)*-**10h** was 3 times more active than the racemic counterpart. For the enantiopure compounds, an antiviral activity similar to or higher than that of **1** was reached. In summary, we identified two new hit compounds as active as pleconaril **1**, in the context of *in vitro* RV-B14 infection. Furthermore, we were able to demonstrate that the HPLC enantioseparation is a mandatory step to significantly improve the antiviral activity and selectivity index of this class of compounds.

Table 2. *In vitro* biological activity of enantiopure compounds against RV-B14.[a]

Entry	Compd	EC_{50} RV-B14 (µM)[b]	CC_{50} HeLa (µM)[c]	SI[d]
1	*(rac)*-**10e**	0.2 ± 0.1	> 1000	> 5000
2	*(S)*-**10e**	0.035 ± 0.006	> 342	> 9771
3	*(R)*-**10e**	2.5 ± 0.9	> 342	> 136
4	*(rac)*-**10h**	0.18 ± 0.05	699 ± 63	3883
5	*(S)*-**10h**	0.06 ± 0.03	> 342	> 5700
6	*(R)*-**10h**	> 128	> 342	-
7	**1**	0.03 ± 0.02	> 131	> 4039

[a] All values are expressed as median ± Med. Abs. Dev. [b] EC_{50} = 50% effective concentration (concentration at which 50% inhibition of virus-induced cell death is observed). [c] CC_{50} = 50% cytotoxic concentration (concentration at which 50% adverse effect is observed on host cell viability). [d] SI = selectivity index for RV-B14, SI = CC_{50}/EC_{50}. *(rac)* = racemic.

Pan-RV activities of 10e and 10h

The antiviral activity of the most promising compounds of the series, compounds **10e** and **10h**, and their enantioseparated counterparts was evaluated against a representative panel of rhinoviruses belonging to type A (RV-A02, RV-A08, RV-A28, RV-A85, and RV-A89), and type B (RV-B14, RV-B42, and RV-B70) (Table 3).

All the compounds were found to be active against RV-group B in a similar range of concentration, with the exception of RV-B42 type, which is known to be naturally resistant to pleconaril-like capsid binders.[46] Interestingly, for the first time, this class of compounds showed antiviral activity against A-group RVs, in particular where RV-A89 infection was involved. Remarkably, in the case of the only type A-virus sensitive to compounds **10e** and **10h**, the *(R)*-enantiomers were more active than the *(S)*-counterparts. This switch in enantiomer activity could reflect specific properties of the pocket. An in-depth study of the primary VP1 sequence highlighted an additional H-bond with the *(R)*-enantiomers (Figure 5).

Table 3. Evaluation of pan-RV activities of the enantiomers of **10e** and **10h**.[a]

Types		EC_{50} **1** (µM)[b]	EC_{50} ***(S)*-10e** (µM)[b]	EC_{50} ***(R)*-10e** (µM)[b]	EC_{50} ***(S)*-10h** (µM)[b]	EC_{50} ***(R)*-10h** (µM)[b]
RV-A	RV-A02	0.015 ± 0.002	> 128	> 128	> 128	> 128
	RV-A08	0.49 ± 0.09	> 128	> 128	> 128	> 128
	RV-A28	0.015 ± 0.008	> 128	> 128	> 128	> 128
	RV-A85	0.011 ± 0.002	> 128	> 128	> 128	> 128
	RV-A89	0.0040 ± 0.0001	2.4 ± 0.5	0.190 ± 0.001	> 128	1.5 ± 0.4
RV-B	RV-B14	0.03 ± 0.02	0.035 ± 0.006	2.5 ± 0.9	0.06 ± 0.03	> 128
	RV-B42	> 128	> 128	> 128	> 128	> 128
	RV-B70	0.167 ± 0.007	0.017 ± 0.006	> 128	0.05 ± 0.03	> 20

[a] All values are expressed as median ± Med. Abs. Dev. [b] EC_{50} = 50% effective concentration (concentration at which 50% inhibition of virus-induced cell death is observed).

10e and 10h act as early-stage inhibitors of Rhinovirus replication.

To confirm the mode of action of the newly-synthetized analogues, a time-of-addition experiment was performed (Figure 2). Compounds **10e** and **10h** and the most active enantioseparated counterparts were added at selected time points before, during, and after infection. Viral replication was quantified 8 hours after infection by the amount of intracellular viral RNA. We observed that both the racemic mixtures of **10e** and **10h** and the purified enantiomers *(S)*-**10e** and *(S)*-**10h** interfered with RV-B14 replication at an early stage. In particular, the compounds were able to prevent virus replication only when added 2 hours before or at the time of infection, which resulted in a decreased intracellular viral RNA load 8 hours after infection. The inhibitory effect of the molecules was completely lost when added 2 or more hours after infection (no reduction in viral RNA load compared to the virus control (VC)) indicating that the compounds act at an early stage of RV replication, similar to **1** and the initial hit **3** (**LPCRW_0005**).[39] These observations indicate that the pharmacomodulations did not alter the mechanism of action of this series of compounds.

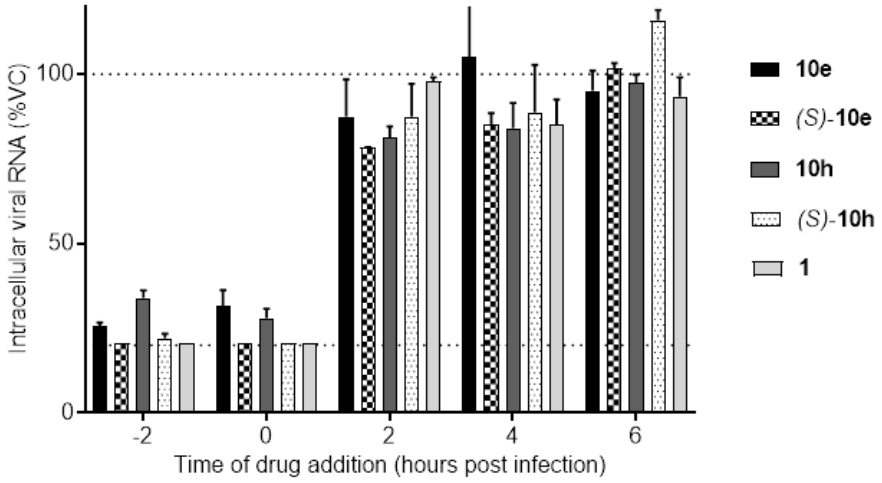

Figure 2. Time of drug-addition experiment. Cells were treated with the compounds **10e**, **10h** and the respective enantiomers at selected time points pre- and post-infection (RV-B14). Pleconaril (**1**) was used as a positive control for early stage inhibition of viral replication. Cells were harvested 8 hours post infection and viral RNA was quantified by RT-qPCR. Similar to **1**, compounds **10e** and **10h** and their active enantiomers interfere with RV-B14 replication at an early stage.

Drug-resistance develops later with compounds 10e and 10h than with pleconaril 1.

The rapid development of resistance against capsid binders such as pleconaril is a major obstacle both *in vitro* and *in vivo*, as demonstrated by several clinical trials. To evaluate the dynamics of emerging resistance, RV-B14 was passaged in the presence of **10e**, **10h** and **1** at their *in vitro* EC_{50}, 2xEC_{50} and 4xEC_{50} (Table 4). In the sub-optimal concentration (*in vitro* EC_{50}), the three compounds developed resistance by passage 3, with **10e**-treated cultures less likely to develop resistance by passage 4 (only 50% of infected-treated cultures showed viral-induced CPE). However, at the higher concentration of 2xEC_{50} and 4xEC_{50}, required for efficacious antiviral treatment, resistance developed more rapidly in **1**-treated than in **10e**- and

10h-treated cultures. Although it is difficult to ultimately conclude on *in vitro* evolutionary experiments, these data may suggest that RV-B14 is less prone to develop resistance in presence of compound **10e** or **10h** than in presence of **1**.

Table 4. RV-B14 induced CPE at passage 1-4 (P1-4) in presence of compounds **10e**, **10h**, or pleconaril **1**.

Compd	xEC_{50}	P1[a]	P2[a]	P3[a]	P4[a]
10e	4	0%	0%	0%	0%
	2	0%	0%	0%	50%
	1	0%	0%	50%	50%
10h	4	0%	0%	0%	0%
	2	0%	0%	25%	50%
	1	0%	50%	75%	100%
1	4	0%	0%	25%	25%
	2	0%	0%	100%	100%
	1	0%	100%	100%	100%
VC		100%	100%	100%	100%

[a]Percentage of wells showing full CPE (n=4). VC: virus control.

Next, in order to correlate the resistant phenotype with eventual drug-resistant virus variants, the VP1 genomic region from the cultures treated with compounds **10e** and **10h** at passage 4 was analyzed by sequencing. Virus harvested from cultures that proved to be equally sensitive to the compound after four passages and without any sign of viral-induced CPE, showed no mutations, except for four (out of 14) cultures that carried either the amino acid substitution A150V or V191E. Both mutations were previously associated with *in vitro* resistance to **1**.[43] On the other hand, the virus harvested from drug-resistant cultures carried one of the mutations A150V, C199W, or N105S. As mentioned above, both A150V but also position C199 (C199Y variant) were previously described for *in vitro* resistance to **1**.[44] The N105S substitution is a new variant associated with **10h** resistance.

Table 5. Mutations detected in the VP1 gene of RV-B14 cultures 1-4 (C1-C4) after 4 passages in presence of compounds **10e** or **10h**.

Compd	xEC$_{50}$	C1	C2	C3	C4
10e	**4**	A150V	A150V	-	-
	2	A150V	A150V	V191E	-
	1	C199W	C199W	-	-
10h	**4**	A150V	-	-	-
	2	N105S	N105S	-	-
	1	C199W	C199W	C199W	C199W

Green: no CPE. Red: full CPE.

***In vitro* genotoxicity study**

A SAR study of the reference compound **3** highlighted the significance of the nitro group: the absence of NO_2[38] or replacement with an amine or chlorine (unpublished data) abolished antiviral activity against RV-B14 (EC_{50} RV-B14 > 306 µM). Indeed, the presence of a nitro group led us to evaluate the potential clastogenic and/or aneugenic activities of the most active enantiomers *(S)*-**10e** and *(S)*-**10h**. The nitroaromatics can be reduced *in vivo* to form several reactive intermediates (nitro radical, nitroso, nitroxyl radical, or aromatic N-oxide). In this research, their genotoxic effects were evaluated using an *in vitro* micronucleus clastogenicity study.[45] This assay detects compounds that damage chromosomes or interfere with the cell division apparatus, producing abnormal DNA fragments. It is currently a prerequisite for future drug development, especially in the framework of research on nitro compounds.

The test was conducted by incubating CHO cells in culture with the test compounds at increasing concentrations (1 µM to 100 µM), with and without metabolic activation. After exposure, the cells were cultured for a specific period of time allowing micronuclei to form in interphase daughter cells in the presence of a blocking agent of cytokinesis (cytochalasin B). The

harvested cells in interphase were subjected to specific staining and analysis for the presence of micronuclei.

All results are presented in Tables A and B (Supporting Information). No significant increase in micronucleated cell rates was observed for any of the non-cytotoxic concentrations, with or without the metabolizing mixture. These findings indicate that compounds *(S)*-**10e** and *(S)*-**10h** did not exert cytogenetic effects on CHO cells in culture, and did not produce metabolites with cytogenetic effects. The negative results for these capsid binders in the *in vitro* micronucleus assay, indicate that they are devoided of clastogenic and/or aneugenic activities under these experimental conditions.

Molecular modelling

The reported derivatives were studied *via* docking experiments to gain insight into the compounds binding mode. The binding pocket was fixed at the capsid site and the computations were carried out according to a previously reported procedure.[40]

First, we evaluated the most profitable ring A position for the introduction of the substituents (R^2) listed in Table 1. The proposed docking poses showed that the compounds bearing the R^2 substituents at position **4** had the better docking score and a binding mode superimposable with that of the reference compounds **1**, **3** and **4a**.

Also, all the newly synthesized compounds were evaluated by docking. The PLANTS proposed binding poses showed that the compounds shared a consistent binding mode, in accordance with the one of the reference compounds **3** and **4a** (Figure 3).

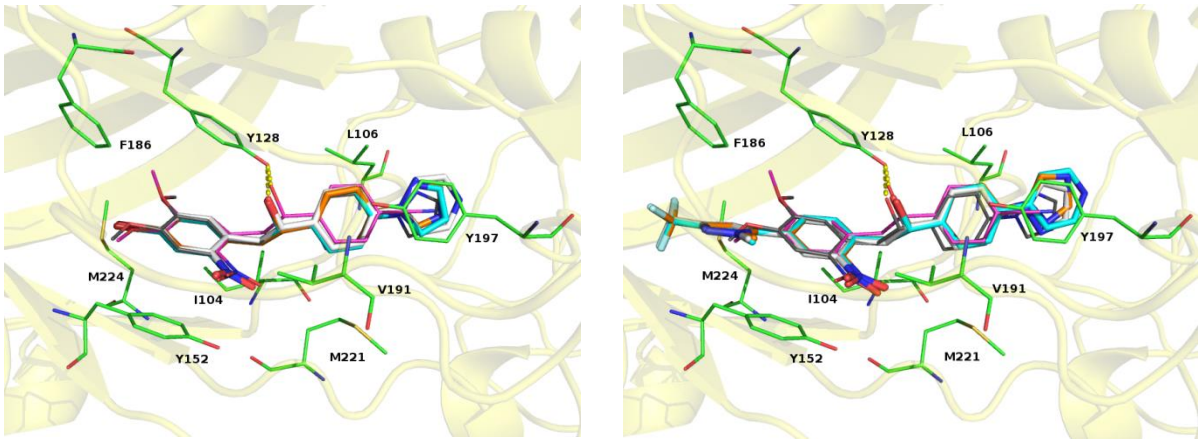

Figure 3. PLANTS proposed binding mode for compounds *(left panel)* **9b** (white), **9c** (orange), and **9f** (cyan); and *(right panel)* **10c** (cyan), **10d** (white), and **10g** (orange). Reference compounds, **3** magenta, and **4a** grey, also depicted as lines. Residues involved in contacts depicted as green lines. VP1 protein depicted as yellow cartoon, H-bonds as yellow dot lines.

The binding mode analyses highlighted some key interactions: (a) the nitro-phenyl moiety had π-π staking with Y152, (b) the linker oxygen atom formed an H-bond with Y128 side chain, and (c) the unsubstituted phenyl ring had hydrophobic interactions with L106, V191 and M221 side chains. The "pore"-side substituents (pyridine, pyrazole, and triazole) were involved in π-π staking contact with Y197. The "toe-end" substituents constituted two distinct groups: the aromatic groups formed staking contact with F186 (Figure 3, *right panel*); whereas the halogen atoms established steric rather than electrostatic interactions at the hydrophobic pocket mainly formed by Y152, F186, and M224 (Figure 3, *left panel*). When compounds **10d**, **10e**, and **10f**, were compared more closely, we observed that the dimethylisoxazole moiety led to an unrelated binding mode, while the CF_3 (**10d**) and the CH_3 (**10e**) groups were superimposable and had hydrophobic contacts with I130, A150, and V176 (Figure D, Supporting Information).

We also studied the binding modes of the **10e** and **10h** enantiomers. The docking poses in particular differed between *(R)* and *(S)* pairs. The *(S)*-enantiomers were in the right geometry to form an H-bond between the chiral oxygen alcohol atom and the Y128 side chain; contrastingly, the alcohol group of the *(R)*-enantiomers pointed toward the hydrophobic residue V191 destabilizing the binding (Figure 4). These findings were in accordance with the biological data and consistent with previously reported docking poses.[41]

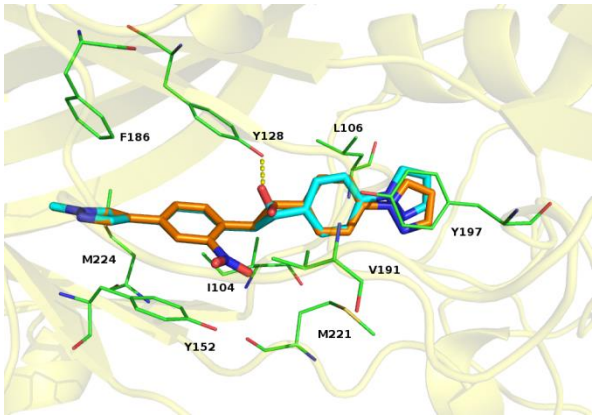

Figure 4. PLANTS proposed binding mode for derivatives *(R)*-**10e** (orange) and *(S)*-**10e** (cyan). Residues involved in contacts depicted as green lines. VP1 protein depicted as yellow cartoon. H-bond is shown as yellow dot line.

The capsid binders integrate into a highly conserved pocket mainly formed by VP1.[46] The serotypes'VP1 primary sequence identities were explored to clarify the broad-range susceptibility of the **10e** and **10h** compounds. Analysis focused on the residues directly involved in interactions with the studied compounds.

For the RV-B studied isotypes (Table 4), comparing RV-B14 and RV-B70 isotypes revealed that only M224 changed to isoleucine. This residue played a role in the stabilization of the compounds making contact with the "toe-end" substituents. Nevertheless, this residue change did

not affect the other contacts and the binding mode (data not shown). Actually, the more hydrophobic nature of the isoleucine might strengthen the interaction with the pyrazole ring. Comparison between RV-B14 and RV-B42 highlighted two residue changes: Y152 to Phe and V191 to Leu. The F152/L191 pattern was previously described as "diagnostic" of resistance to capsid binders.[46] In particular, the bulkier leucine instead of valine might have a detrimental steric effect on compound binding. This hypothesis was confirmed by docking studies with the homology model for RV-B42 VP1. Indeed, the docking experiments for **10e** and **10h** led to an unrelated binding mode (data not shown).

Table 4. VP1 alignment of the amino acids of RV-B types in the binding pocket.

	Amino acid position																					
RV-B	102	104	106	116	124	126	128	150	151	152	174	175	176	186	188	191	197	198	219	221	224	245
14	W	I	L	L	F	S	Y	A	M	Y	P	S	V	F	V	V	Y	N	N	M	M	H
42	-	-	-	-	-	-	-	-	-	F	-	-	-	-	-	L	-	-	-	-	-	-
70	-	-	-	-	-	-	-	-	-	-	-	-	-	-	-	-	-	-	-	-	I	-

We also analyzed the VP1 sequence for the RV-A isotypes (Table 5), aiming to elucidate the great inhibitory activity of **10e** and **10h** on the A89 isotype. It is noteworthy that the valine 98 was peculiar to A89 isotype, and this residue was in the central part of the canyon. The docking experiments with the RV-A89 VP1 homology model confirmed the role of V98. The smaller valine instead of the isoleucine, of the other studied isotypes, created a small space filled by the nitro group. This binding mode also featured in: (a) an aromatic contact between the "pore"-side pyrazole and Y190; (b) a hydrophobic interaction between the "toe-end" pyrazole and F179 and I217; and (c) a contact formed by the nitro-phenyl group with Y144 and I181. It should be noted that the reported binding mode showed an H-bond with the S120 side chain for the *(R)*-enantiomers alone (Figure 5).

Table 5. VP1 alignment of the amino acids of RV-A types in the binding pocket.

	Amino acid position																					
RV-A	77	96	98	100	118	120	122	124	142	143	144	166	167	168	179	181	184	190	212	214	217	238
89	I	W	V	L	F	S	I	I	F	M	Y	A	S	V	F	I	M	Y	N	M	I	H
2	-	-	I	-	-	-	-	L	Y	-	-	-	-	-	-	L	L	-	-	-	L	-
8	-	-	I	I	-	-	-	-	I	-	-	-	-	-	-	-	S	-	-	-	-	L
28	-	-	I	-	-	-	-	-	-	-	-	-	-	-	-	-	-	-		-	L	-
85	-	-	I	I	-	-	-	L	Y	-	-	-	-	-	-	-	-	-	-	-	L	-

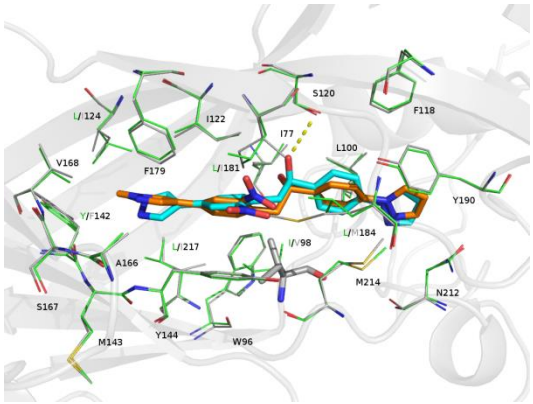

Figure 5. Proposed binding mode for the compounds *(R)*-**10e** (cyan) and *(S)*-**10e** (orange) at RV-A89 isotype. Residues of RV-A2 depicted as green lines; residues of RV-A89 depicted as grey lines. The cartoon of A89 isotype is also shown. H-bond shown as yellow dot line.

The docking studies provided us with a general binding mode consistent with the biological activity. Nevertheless, several other factors might be involved in the compound binding, such as: the effect of other changed amino acids, the residues outside the binding pocket and the compounds' access to the pocket.

DISCUSSION

Capsid binders are still considered attractive molecules for the prophylaxis and treatment of rhino/enterovirus infections, as witnessed by the wealth of studies/clinical trials over the recent years. These molecules target the hydrophobic pocket beneath the floor of the canyon formed by

approximately twenty amino acids of VP1. This viral protein is highly variable across Rhinoviruses and Enteroviruses as well as the composition of the pocket. It is hence a challenge to design molecules that are strong capsid binders and pan-genotype active. Here, we describe the chemical modulation of a pleconaril-like capsid binder with greater *in vitro* antiviral activity than that of **3** and **4** and a broader spectrum of activity against Rhinoviruses.

Following enantioseparation, *(S)*-**10h** showed just a high potency against RV-B14 infection and an increased potency compared to **1** against RV-B70 infection. In addition, both the **10e** and **10h** exhibited a delayed *in vitro* resistance development compared to **1**. Although the interpretation of *in vitro* evolutionary experiments is challenging, our data suggest that RV-B14 is likely less prone to develop resistance in presence of compounds **10e** and **10h** than in presence of **1**. As resistance development was a major problem during the clinical development phase of **1**, our findings on this novel class of pleconaril-like compounds are highly encouraging. Moreover, we correlated the resistance phenotype with mutations in VP1. Two of the altered positions (A150 and C199) were previously associated with resistance to **1**, whereas N105S is a newly-identified variant specifically associated with compound **10h** and/or **10e**. These residues lie in close proximity to the residues defining the hydrophobic pocket, suggesting that the environment around the pocket is also crucial for compound-binding.

This study also shed light on the dynamics of interaction of the newly-synthesized x-analogues with the binding pocket by means of molecular docking simulations. We were able to identify the residue V98 in RV-A as a key residue associated with *in vitro* antiviral activity. In addition, the differing enantiomer preferences in the context of RV-B or RV-A89 infection are explained. Only the *(R)*-enantiomer was able to engage in an H-bond with the pocket residue S120,

suggesting that this residue is also crucial for antiviral activity. Taken together, these data will guide the synthesis of more potent and broad-spectrum compounds.

CONCLUSION

In summary, we identified a novel RV inhibitors series with a promising pharmacological profile. Several compounds displayed sub-micromolar EC_{50} values against a representative panel of RV species. In line with our previous work, this SAR study was undertaken to lengthen our scaffold on the closed side of the hydrophobic pocket, called the "toe-end". This work confirms the value of hydrophobic interactions with the residues I130, A150, and V176 from the “toe-end” side. Several structures were identified, among them methyl pyrazole compounds showed to form numerous hydrophobic interactions within the pocket. The enantiopure compounds **10e** and **10h** inhibited replication of RV-A and RV-B species with an EC_{50} between 0.017 and 0.19 μM against RV-B14, RV-B70 and RV-A89, and were comparable to **1**. Determination of the absolute configuration *via* Mosher’s protocol confirms the major role played by the *(S)*-alcohol linker against RV-B14 and RV-B70. Conversely, the *(R)*-stereocenter of **10e** induced activity against RV-A89. The docking studies showed that an H-bond with S120 plays a key role for this activity.

The results of time-of-addition experiments, in which *(S)*-**10e** and *(S)*-**10h** show an inhibition profile similar to that of **1** against RV-B14, and of a resistance-development study, indicate that compounds **10** act at an early stage of the viral infection. In addition, a new point mutation N105S on the viral capsid protein is identified. Our *in vitro* genotoxicity study also reveals that derivatives **10** have no clastogenic and/or aneugenic activities in CHO cells, despite the nitro group. In conclusion, this full-ranging investigation identifies two potent antivirals with broad-

spectrum activity against RV-A and RV-B species. In view of their promising pharmacological properties, we therefore intend to explore the pan-EV potential of these new pyrazole inhibitors.

EXPERIMENTAL SECTION

Chemistry

*General methods***.** Commercially available reagents and solvents were used without further purification. Reactions were monitored by thin-layer chromatography (plates coated with silica gel 60 F_{254} from Merck) and by LC-MS analyses with a Thermo Scientific Accela High Speed LC System® coupled with a single quadrupole mass spectrometer Thermo MSQ Plus®. The RP-HPLC column used is a Thermo Hypersil Gold® 50 x 2.1 mm (C18 bounded), with particles of 1.9 µm diameter. Analysis was 8 min running with a MeOH/H_2O eluent gradient from 50:50 to 95:05. Silica gel 60 (70-230 mesh from Macherey-Nagel) was used for flash chromatography. Melting points were measured in open capillary tubes with Büchi apparatus and are uncorrected. ^{1}H and ^{13}C NMR spectra were recorded at room temperature in deuterated solvents on a Brüker Avance-250 instrument (250 MHz), a Brüker Avance III nanobay-300 MHz or a Brüker Avance III nanobay-400 MHz. Chemical shifts (δ) are reported in parts per million (ppm) relative to TMS as internal standard or relative to the solvent [^{1}H: δ(DMSO) = 2.50 ppm, δ($CDCl_3$) = 7.26 ppm; ^{13}C: δ(DMSO) = 39.52 ppm, δ($CDCl_3$) = 77.16 ppm]. Data are reported as follows: chemical shift, multiplicity (s = singulet, d = doublet, t = triplet, q = quartet, dd = doublet of doublets, m = multiplet, and bs = broad singlet), coupling constant in Hertz, and integration. Two-dimensional spectroscopy (HSQC and HMBC) was used to assist in the assignment and the data are not reported. Accurate mass measurements (HRMS) were recorded on a TOF spectrometer, realized by Spectropôle of Faculté des Sciences de Saint Jérôme, Marseille

(France). Purity of tested compounds was found to be > 95% by high pressure liquid chromatography (HPLC).

4-Bromo-1-(chloromethyl)-2-nitrobenzene (6a). Step 1: BH_3 (1.0 M solution in THF, 7 mL, 7 mmol) was slowly added to a solution of 4-bromo-2-nitrobenzoic acid (2 g, 8.1 mmol) in anhydrous THF (10 mL) at 0 °C. The mixture was stirred at room temperature for 3 days. The mixture was quenched by dropwise addition of a saturated aqueous solution of $NaHCO_3$. Then, the mixture was extracted with ethyl acetate. The combined organic layers were washed with water and brine, dried over anhydrous Na_2SO_4, filtered off and concentrated under reduced pressure to afford the pure (4-bromo-2-nitrophenyl)methanol (1.3 g, 5.7 mmol, yield *71 %*) as a beige solid. Step 2: To a solution of (4-bromo-2-nitrophenyl)methanol (1.3 g, 5.7 mmol) in CH_2Cl_2 (10 mL) was added a few drops of triethylamine, and $SOCl_2$ (0.5 mL, 6.7 mmol) at 0 °C. After stirring overnight at room temperature, the reaction was quenched by addition of an aqueous solution NaOH 2N. The mixture was washed with water and brine, dried over anhydrous Na_2SO_4, filtered off and concentrated under reduced pressure. After purification by column chromatography on silica gel (Petroleum ether/EtOAc 8:2), the pure product **6a** (1,3 g, 5,2 mmol, yield *92%*) was obtained as a beige solid. ^{1}H NMR (250 MHz, $CDCl_3$) δ 8.21 (d, J = 1.7 Hz, 1H), 7.77 (dd, J = 8.3, 1.7 Hz, 1H). 7.59 (d, J = 8.3 Hz, 1H), 4.93 (s, 2H, CH_2). ^{13}C NMR (62.5 MHz, $CDCl_3$) δ 148.4 ($C_{IV,Ar}$), 136.9 (CH_{Ar}), 133.0 (CH_{Ar}), 131.6 ($C_{IV,Ar}$), 128.4 (CH_{Ar}), 122.8 ($C_{IV,Ar}$), 42.3 (CH_2).

4-Chloro-1-(chloromethyl)-2-nitrobenzene (6b). Synthesized following the same procedure used to prepare **6a**, the crude product was prepared with 4-chloro-2-nitrobenzoic acid (2.3 g, 11.4 mmol). After purification by column chromatography on silica gel (CH_2Cl_2), the pure product **6b** (2.14 g, 10.4 mmol, yield *92%*) was obtained as a brown oil. ^{1}H NMR (250 MHz, $CDCl_3$) δ 8.00

(d, J = 1.6 Hz, 1H), 7,65-7,57 (m, 2H), 4,91 (s, 2H, CH_2). ^{13}C NMR (62.5 MHz, $CDCl_3$) δ 148,2 ($C_{IV,Ar}$), 135,3 ($C_{IV,Ar}$), 133,8 (CH_{Ar}), 132,8 (CH_{Ar}), 131,0 ($C_{IV,Ar}$), 125,4 (CH_{Ar}), 42,2 (CH_2).

4-Fluoro-1-(chloromethyl)-2-nitrobenzene (6c). Synthesized following the same procedure used to prepare **6a**, the crude product was prepared with 4-fluoro-2-nitrobenzoic acid (1.3 g, 7.0 mmol). After purification by column chromatography on silica gel (CH_2Cl_2), the pure product **6c** (1.16 g, 6.1 mmol, yield *89%*) was obtained as a green oil. ^{1}H NMR (250 MHz, $CDCl_3$) δ 7,75 (dd, J_{HF} = 8.2 Hz, J_{HH} = 2.7 Hz, 1H), 7,68 (dd, J_{HH} = 8.6 Hz, J_{HF} = 5.4 Hz, 1H), 7,40-7,33 (m, 1H), 4,91 (s, 2H, CH_2). ^{13}C NMR (62.5 MHz, $CDCl_3$) δ 161.9 (d, $^1J_{CF}$ = 251 Hz, $C_{IV,Ar}$), 148.4 (d, $^3J_{CF}$ =8 Hz, $C_{IV,Ar}$), 133.5 (d, $^3J_{CF}$ = 8 Hz, CH_{Ar}), 128.6 (d, $^4J_{CF}$ = 4 Hz, $C_{IV,Ar}$), 121.1 (d, $^2J_{CF}$ = 21 Hz, CH_{Ar}), 113.0 (d, $^2J_{CF}$ = 27 Hz, CH_{Ar}), 42.2 (CH_2).

Methyl 4-(chloromethyl)-3-nitrobenzoate (6d). Synthesized following the same procedure used to prepare **6a**, 4-(methoxycarbonyl)-2-nitrobenzoic acid (1.0 g, 4.4 mmol) was used to obtain the pure product **6d** (903 mg, 3.9 mmol, yield *79%*) as a brown oil. ^{1}H NMR (250 MHz, $CDCl_3$) δ 8.61 (d, J = 1.7 Hz, 1H), 8.24 (dd, J = 8.0, 1.7 Hz, 1H), 7.79 (d, J = 8.0 Hz, 1H), 4.97 (s, 2H, CH_2), 3.95 (s, 3H, CH_3). ^{13}C NMR (62.5 MHz, $CDCl_3$) δ 164.5 (C=O), 147.9 ($C_{IV,Ar}$), 136.7 ($C_{IV,Ar}$), 134.2 (CH_{Ar}), 131.9 (CH_{Ar}), 131.6 ($C_{IV,Ar}$), 126.2 (CH_{Ar}), 52.9 (CH_3), 42.4 (CH_2).

General procedure A for the synthesis of 9. To a glass vessel suitable for sealing with Teflon cap (for microwave vials) were added the benzyl chloride derivative **6a-6d** (1 equiv.) and benzaldehyde derivative (3 equiv.). The vessel was capped and then evacuated and backfilled with N_2 (thrice-repeated process). Anhydrous DMF (3.5 mL/mmol) was introduced and the solution was vigorously stirred for 20 min at -20 °C. TDAE (1.06 equiv.) was added slowly and the mixture was stirred for one hour. Then, the reaction was stirred at room temperature

overnight. After LC-MS analysis clearly showed that the chloride had been totally consumed, the reaction was hydrolyzed with water. The mixture was then extracted with ethyl acetate. The combined organic layers were washed with water and brine, dried over anhydrous Na_2SO_4, filtered off, and concentrated under reduced pressure to afford the corresponding crude product.

Methyl 4-(2-hydroxy-2-(4-(pyridin-4-yl)phenyl)ethyl)-3-nitrobenzoate (9a). The crude product was prepared according to procedure A starting from **6d** (100 mg, 0.43 mmol) and **8** (239 mg, 1.30 mmol). After purification by column chromatography on silica gel (CH_2Cl_2/Diethyl ether 9:1 to 6:4), the pure product **9a** (64 mg, 0.17 mmol, yield *39%*) was obtained as a yellow solid. m.p: 188 °C. ^{1}H NMR (400 MHz, DMSO-d_6) δ 8.62 (d, J = 6.1 Hz, 2H), 8.37 (d, J = 1.6 Hz, 1H), 8.15 (dd, J = 8.1, 1.6 Hz, 1H), 7.79 (d, J = 8.2 Hz, 2H), 7.71 (d, J = 6.1 Hz, 2H), 7.67 (d, J = 8.1 Hz, 1H), 7.47 (d, J = 8.2 Hz,2H), 5.59 (d, J = 4.7 Hz, 1H, O*H*), 4.88-4.84 (m, 1H), 3.90 (s, 3H, CH_3), 3.31-3.24 (m, 2H). ^{13}C NMR (100 MHz, DMSO-d_6) δ 164.6 (C=O), 150.2 (2xCH_{Ar}), 150.0 ($C_{IV,Ar}$), 146.7 ($C_{IV,Ar}$), 146.2 ($C_{IV,Ar}$), 138.4 (CH_{Ar}), 135.8 ($C_{IV,Ar}$), 134.2 ($C_{IV,Ar}$), 132.4 (CH_{Ar}), 129.0 ($C_{IV,Ar}$), 126.6 (2xCH_{Ar}), 126.4 (2xCH_{Ar}), 124.6 (CH_{Ar}), 121.0 (2xCH_{Ar}), 72.0 (CH), 52.6 (CH_3), 41.6 (CH_2). HRMS (ESI+) m/z Calc. for $C_{21}H_{18}N_2O_5$ $[M+H]^+$ 379.1288, found 379.1288.

2-(4-Bromo-2-nitrophenyl)-1-(4-(pyridin-4-yl)phenyl)ethanol (9b). The crude product was prepared according to procedure A starting from **6a** (500 mg, 1.99 mmol) and **8** (1097 mg, 5.98 mmol). After purification by column chromatography on silica gel (EtOAc/Cyclohexane 6:4 to 7:3), the pure product **9b** (215 mg, 0.54 mmol, yield *27%)* was obtained as light a yellow solid. m.p: 177 °C. ^{1}H NMR (300 MHz, DMSO-d_6) δ 8.62 (d, J = 5.8 Hz, 2H), 8.11 (d, J = 1.8 Hz, 1H), 7.82 (dd, J = 8.3, 1.8 Hz, 1H), 7.78 (d, J = 8.1 Hz, 2H), 7.70 (d, J = 5.8 Hz, 2H), 7.46 (d, J = 8.3 Hz, 1H), 7.45 (d, J = 8.1 Hz, 2H), 5.53 (d, J = 4.7 Hz, 1H, O*H*), 4.84-4.78 (m, 1H), 3,23-3,10

(m, 2H). ^{13}C NMR (75 MHz, DMSO-d$_6$) δ 150.7 ($C_{IV,Ar}$), 150.2 (2xCH_{Ar}), 146.7 ($C_{IV,Ar}$), 146.2 ($C_{IV,Ar}$), 135.8 ($C_{IV,Ar}$), 135.2 (CH_{Ar}), 135.1 ($C_{IV,Ar}$), 132.3 ($C_{IV,Ar}$), 126.6 (2xCH_{Ar}), 126.5 ($C_{IV,Ar}$), 126.4 (2xCH_{Ar}), 121.0 (2xCH_{Ar}), 119.3 (CH_{Ar}), 71.9 (CH_{Ar}), 40.9 (CH_2). HRMS (ESI+) m/z Calc. for $C_{19}H_{15}BrN_2O_3$ $[M+H]^+$ 399.0339, found 399.0339.

1-(4-(1*H*-Pyrazol-1-yl)phenyl)-2-(4-bromo-2-nitrophenyl)ethanol (9c). The crude product was prepared according to procedure A starting from **6a** (500 mg, 1.99 mmol) and 4-(1*H*-pyrazol-1-yl)benzaldehyde (1031 mg, 5.98 mmol). After purification by column chromatography on silica gel (Petroleum ether/EtOAc 7:3), the pure product **9c** (230 mg, 0.59 mmol, yield *30%*) was obtained as a light orange solid. m.p: 164 °C. ^{1}H NMR (400 MHz, DMSO-d$_6$) δ 8.47 (d, J = 2.6 Hz, 1H), 8.10 (d, J = 2.0 Hz, 1H), 7.82 (dd, J = 8.3, 2.0 Hz, 1H), 7.79 (d, J = 8.6 Hz, 2H), 7.73 (d, J = 1.5 Hz, 1H), 7.42 (d, J = 8.3 Hz, 1H), 7.41 (d, J = 8.6 Hz, 2H), 6.53 (dd, J = 2.6, 1.5 Hz, 1H), 5.54 (d, J = 4,6 Hz, 1H, O*H*), 4.80-4.76 (m, 1H), 3.17-3.15 (m, 2H). ^{13}C NMR (100 MHz, DMSO-d$_6$) δ 150.7 ($C_{IV,Ar}$), 142.8 ($C_{IV,Ar}$), 140.8 (CH_{Ar}), 138.7 ($C_{IV,Ar}$), 135.2 ($C_{IV,Ar}$), 135.1 (CH_{Ar}), 132.3 (CH_{Ar}), 127.6 (CH_{Ar}), 126.7 (2xCH_{Ar}), 126.5 ($C_{IV,Ar}$), 119.4 (CH_{Ar}), 118.0 (2xCH_{Ar}), 107.7 (CH_{Ar}), 71.8 (CH), 40.1 (CH_2). HRMS (ESI+) m/z Calc. for $C_{17}H_{14}BrN_3O_3$ $[M+H]^+$ 388.0291, found 388.0294.

1-(4-(1*H*-Pyrazol-1-yl)phenyl)-2-(4-chloro-2-nitrophenyl)ethanol (9d). The crude product was prepared according to procedure A starting from **6b** (200 mg, 0.97 mmol) and 4-(1*H*-pyrazol-1-yl)benzaldehyde (251 mg, 1.45 mmol, 1.5 equiv.). After purification by column chromatography on silica gel (Petroleum ether/EtOAc 8:2 to 5:5), the pure product **9d** (68 mg, 0.19 mmol, yield *20%*) was obtained as light a yellow solid. m.p: 167 °C. ^{1}H NMR (250 MHz, DMSO-d$_6$) δ 8.48 (d, J = 2.4 Hz, 1H), 8.01 (d, J = 2.2 Hz, 1H), 7.79 (d, J = 8.4 Hz, 1H), 7.73 (d, J = 8.6 Hz, 2H), 7.69 (d, J = 2.2 Hz, 1H), 7.47 (d, J = 8.4 Hz, 1H), 7.38 (d, J = 8.6 Hz, 2H), 6.54

(dd, J = 2.4, 2.2 Hz, 1H), 5.56 (d, J = 4.5 Hz, 1H, O*H*), 4.82-4.75 (m, 1H), 3.22-3.17 (m, 2H). ^{13}C NMR (75 MHz, DMSO-d_6) δ 150.5 ($C_{IV,Ar}$), 142.8 ($C_{IV,Ar}$), 140.7 (CH_{Ar}), 138.6 ($C_{IV,Ar}$), 134.9 (CH_{Ar}), 132.3 ($C_{IV,Ar}$), 131.9 (CH_{Ar}), 131.5 ($C_{IV,Ar}$), 127.5 (CH_{Ar}), 126.7 (2xCH_{Ar}), 123.7 (CH_{Ar}), 118.0 (2xCH_{Ar}), 107.6 (CH_{Ar}), 71.8 (CH), 40.9 (CH_2). HRMS (ESI+) m/z Calc. for $C_{17}H_{14}ClN_3O_3$ $[M+H]^+$ 344.0796, found 344.0795.

1-(4-(1*H*-Pyrazol-1-yl)phenyl)-2-(4-fluoro-2-nitrophenyl)ethanol (9e). The crude product was prepared according to procedure A starting from **6c** (200 mg, 1.05 mmol) and 4-(1*H*-pyrazol-1-yl)benzaldehyde (273 mg, 1.58 mmol, 1.5 equiv.). After purification by column chromatography on silica gel (Petroleum ether/EtOAc 8:2 to 5:5), the pure product **9e** (120 mg, 0.36 mmol, yield *35%*) was obtained as light a yellow solid. m.p: 145 °C. ^{1}H NMR (250 MHz, DMSO-d_6) δ 8.48 (d, J = 2.3 Hz, 1H), 7.85 (dd, J = 8.9, 2.4 Hz, 1H), 7.79 (d, J = 8.5 Hz, 2H), 7.73 (d, J = 1.5 Hz, 1H), 7.58-7.46 (m, 2H), 7.39 (d, J = 8.5 Hz, 2H), 6.53 (dd, J = 2.3, 1.5 Hz, 1H), 5.53 (d, J = 4.6 Hz, 1H, O*H*), 4.81-4.74 (m, 1H), 3.19-3.17 (m, 2H). ^{13}C NMR (62.5 MHz, DMSO-d_6) δ 159.9 (d, $^1J_{CF}$ = 245 Hz, $C_{IV,Ar}$), 150.4 (d, $^3J_{CF}$ = 8 Hz, $C_{IV,Ar}$), 143.0 ($C_{IV,Ar}$), 140.8 (CH_{Ar}), 138.7 ($C_{IV,Ar}$), 135.2 (d, $^3J_{CF}$ = 8 Hz, CH_{Ar}), 129.3 (d, $^4J_{CF}$ = 4 Hz, $C_{IV,Ar}$), 127.6 (CH_{Ar}), 126.7 (2xCH_{Ar}), 119.8 (d, $^2J_{CF}$ = 21 Hz, CH_{Ar}), 118.0 (2xCH_{Ar}), 111.5 (d, $^2J_{CF}$ = 26 Hz, CH_{Ar}), 107.8 (CH_{Ar}), 72.0 (CH), 40.9 (CH_2). HRMS (ESI+) m/z Calc. for $C_{17}H_{14}FN_3O_3$ $[M+H]^+$ 328.1092, found 328.1090.

1-(4-(1*H*-1,2,4-Triazol-1-yl)phenyl)-2-(4-bromo-2-nitrophenyl)ethanol (9f). The crude product was prepared according to procedure A starting from **6a** (500 mg, 1.99 mmol) and 4-(1*H*-1,2,4-triazol-1-yl)benzaldehyde (1037 mg, 5.98 mmol). After purification by column chromatography on silica gel (EtOAc/Petroleum ether 8:2), the pure product **9f** (101 mg, 0.26 mmol, yield *13%)* was obtained as a yellow solid. m.p: 192 °C. ^{1}H NMR (250 MHz, DMSO-d_6)

δ 9.29 (s, 1H), 8.23 (s, 1H), 8.11 (d, J = 2,1 Hz, 1H), 7.83 (dd, J = 8.3, 2.1 Hz, 1H), 7.82 (d, J = 8.6 Hz, 2H), 7.47 (d, J = 8.6 Hz, 2H), 7,42 (d, J = 8.3 Hz, 1H), 5,61 (d, J = 4.7 Hz, 1H, O*H*), 4.84-4.77 (m, 1H), 3.18-3.15 (m, 2H). ^{13}C NMR (100 MHz, DMSO-d_6) δ 152.3 (CH_{Ar}), 150.7 ($C_{IV,Ar}$), 144.6 (CH_{Ar}), 142.2 ($C_{IV,Ar}$), 135.6 ($C_{IV,Ar}$), 135.2 ($C_{IV,Ar}$), 135.1 (CH_{Ar}), 132.2 (CH_{Ar}), 126.9 (2xCH_{Ar}), 126.5 ($C_{IV,Ar}$), 119.4 (CH_{Ar}), 119.1 (2xCH_{Ar}), 71.7 (CH), 40.9 (CH_2). HRMS (ESI+) m/z Calc. for $C_{16}H_{13}BrN_4O_3$ $[M+H]^+$ 389.0244, found 389.0242.

General procedure B for the synthesis of 10a-10c. To a sealed glass vial were added the brominated derivative (1 equiv.), boronic acid derivative (2 equiv.), $Pd(PPh_3)_2Cl_2$ (3 mol%), and K_2CO_3 (2 equiv.). The vessel was capped and then, evacuated and backfilled with N_2 (process repeated 3X). The dioxane (8 mL/mmol) was introduced and the solution was heated at 80 °C overnight. After cooling, the mixture was extracted with ethyl acetate. The combined organic layers were washed with water and brine, dried over anhydrous Na_2SO_4, filtered off, and concentrated under reduced pressure to afford the corresponding crude product **10a-10c**.

2-(2-Nitro-4-(thiophen-2-yl)phenyl)-1-(4-(pyridin-4-yl)phenyl)ethanol (10a). The crude product was prepared according to procedure B starting from **9b** (80 mg, 0.20 mmol) and thiophen-2-ylboronic acid (52 mg, 0.40 mmol). After purification by column chromatography on silica gel (Petroleum ether/EtOAc 7:3), the pure product **10a** (53 mg, 0.13 mmol, yield *66%*) was obtained as a light yellow solid. m.p: 217 °C. ^{1}H NMR (300 MHz, DMSO-d_6) δ 8.62 (d, J = 3.4 Hz, 2H), 8.13 (s, 1H), 7.90-7.64 (m, 7H), 7.53-7.46 (m, 3H), 7.19-7.17 (m, 1H), 5.53 (d, J = 4.9 Hz, 1H, O*H*), 4.89-4.79 (m, 1H), 3.26-3.13 (m, 2H). ^{13}C NMR (75 MHz, DMSO-d_6) δ 150.6 ($C_{IV,Ar}$), 150.2 (2xCH_{Ar}), 146.7 ($C_{IV,Ar}$), 146.4 ($C_{IV,Ar}$), 140.6 (CH_{Ar}), 135.7 ($C_{IV,Ar}$), 134.1 ($C_{IV,Ar}$), 133.2 (CH_{Ar}), 131.8 ($C_{IV,Ar}$), 128.9 ($C_{IV,Ar}$), 128.7 (CH_{Ar}), 126.9 (CH_{Ar}), 126.5

(2xCH_{Ar}), 126.4 (2xCH_{Ar}), 125.3 (CH_{Ar}), 121.0 (2xCH_{Ar}), 120.2 (CH_{Ar}), 72.1 (CH), 41.3 (CH_2). HRMS (ESI+) m/z Calc. for $C_{23}H_{18}N_2O_3S$ $[M+H]^+$ 403.1111, found 403.1105.

2-(4-(Furan-2-yl)-2-nitrophenyl)-1-(4-(pyridin-4-yl)phenyl)ethanol (10b). The crude product was prepared according to procedure B starting from **9b** (80 mg, 0.20 mmol) and furan-2-ylboronic acid (45 mg, 0.40 mmol). After purification by column chromatography on silica gel (Petroleum ether/EtOAc 7:3), the pure product **10b** (56 mg, 0.14 mmol, yield *73%*) was obtained as an orange solid. m.p: 219 °C. ^{1}H NMR (300 MHz, DMSO-d_6) δ 8.62 (d, J = 5.7 Hz, 2H), 8.15 (d, J = 1.5 Hz, 1H), 7.91 (dd, J = 8.0, 1.5 Hz, 1H), 7,81 (d, J = 1.7 Hz, 1H), 7.78 (d, J = 8.1 Hz, 2H), 7.70 (d, J = 5.7 Hz, 2H), 7.52 (d, J = 8.0 Hz, 1H), 7.47 (d, J = 8.1 Hz, 2H), 7.14 (d, J = 3.2 Hz, 1H), 6.65 (dd, J = 3.2, 1.7 Hz, 1H), 5.53 (d, J = 4,7 Hz, 1H, O*H*), 4,88-4,82 (m, 1H), 3.27-3.15 (m, 2H). ^{13}C NMR (75 MHz, DMSO-d_6) δ 150.8 ($C_{IV,Ar}$), 150.5 ($C_{IV,Ar}$), 150.2 (2xCH_{Ar}), 146.7 ($C_{IV,Ar}$), 146.4 ($C_{IV,Ar}$), 143.8 (CH_{Ar}), 135.7 ($C_{IV,Ar}$), 134.0 ($C_{IV,Ar}$), 131.6 (CH_{Ar}), 129.6 (CH_{Ar}), 126.8 ($C_{IV,Ar}$), 126.5 (2xCH_{Ar}), 126.4 (2xCH_{Ar}), 121.0 (2xCH_{Ar}), 118.4 (CH_{Ar}), 112.3 (CH_{Ar}), 107.8 (CH_{Ar}), 72.1 (CH), 41.3 (CH_2). HRMS (ESI+) m/z Calc. for $C_{23}H_{18}N_2O_4$ $[M+H]^+$ 387.1339, found 387.1338.

2-(4-(1-Methyl-3-(trifluoromethyl)-1*H*-pyrazol-5-yl)-2-nitrophenyl)-1-(4-(pyridin-4-yl)phenyl)ethanol (10c). The crude product was prepared according to procedure B starting from **9b** (80 mg, 0.20 mmol) and (1-methyl-3-trifluoromethyl-1*H*-pyrazol-5-yl)boronic acid (78 mg, 0,40 mmol). After purification by column chromatography on silica gel (Petroleum ether/EtOAc 5:5), the pure product **10c** (73 mg, 0.16 mmol, yield *78%*) was obtained as a yellow solid. m.p: 151 °C. ^{1}H NMR (300 MHz, DMSO-d_6) δ 8.63 (d, J = 4.8 Hz, 2H), 8.14 (s, 1H), 7.87 (d, J = 7.5 Hz, 1H), 7.80 (d, J = 7.9 Hz, 2H), 7.72-7.67 (m, 3H), 7.51 (d, J = 7.9 Hz, 2H), 7.06 (s, 1H), 5.57 (d, J = 4.5 Hz, 1H, O*H*), 4.89-4.87 (m, 1H), 3.97 (s, 3H, CH_3), 3.27-3.24

(m, 2H). ^{13}C NMR (75 MHz, DMSO-d$_6$) δ 150.3 ($C_{IV,Ar}$), 150.2 (2xCH_{Ar}), 146.7 ($C_{IV,Ar}$), 146.4 ($C_{IV,Ar}$), 142.5 ($C_{IV,Ar}$), 139.7 (q, $^2J_{CF}$ = 37 Hz, $C_{IV,Ar}$), 135.8 ($C_{IV,Ar}$), 133.9 ($C_{IV,Ar}$), 133.9 (CH_{Ar}), 132.3 (CH_{Ar}), 127.9 ($C_{IV,Ar}$), 126.6 (2xCH_{Ar}), 126.4 (2xCH_{Ar}), 124.0 (CH_{Ar}), 121.4 (q, $^1J_{CF}$ = 266 Hz, CF_3), 121.0 (2xCH_{Ar}), 105.1 (q, $^3J_{CF}$ = 2 Hz, CH_{Ar}), 72.1 (CH_{Ar}), 41.3 (CH_2), 38.4 (CH_3). HRMS (ESI+) m/z Calc. for $C_{24}H_{19}F_3N_4O_3$ $[M+H]^+$ 469.1482, found 469.1480.

General procedure C for the synthesis of 10d-10j. To a sealed glass vial were added the brominated derivative (1 equiv.), boronic acid derivative (2 equiv.), Pd(dppf)Cl_2 (5 mol%), and K_2CO_3 (2 equiv.). The vessel was capped and then, evacuated and backfilled with N_2 (process repeated 3X). The dioxane (8 mL/mmol) was introduced and the solution was heated at 80 °C overnight. After cooling, the mixture was extracted with ethyl acetate. The combined organic layers were washed with water and brine, dried over anhydrous Na_2SO_4, filtered off, and concentrated under reduced pressure to afford the corresponding crude product **10d-10j**.

1-(4-(1*H*-Pyrazol-1-yl)phenyl)-2-(4-(1-methyl-3-(trifluoromethyl)-1*H*-pyrazol-5-yl)-2-nitrophenyl)ethanol (10d). The crude product was prepared according to procedure C starting from **9c** (94 mg, 0.24 mmol) and (1-methyl-3-trifluoromethyl-1*H*-pyrazol-5-yl)boronic acid (93 mg, 0.48 mmol). After purification by column chromatography on silica gel (Petroleum ether/EtOAc 5:5), the pure product **10d** (92 mg, 0.20 mmol, yield *84%*) was obtained as a white solid. m.p: 153 °C. ^{1}H NMR (300 MHz, DMSO-d$_6$) δ 8.46 (d, *J* = 2.4 Hz, 1H), 8.13 (d, *J* = 1.6 Hz, 1H), 7.86 (dd, *J* = 8.0, 1.6 Hz, 1H), 7.80 (d, *J* = 8.5 Hz, 2H), 7.73 (d, *J* = 1.3 Hz, 1H), 7.64 (d, *J* = 8.0 Hz, 1H), 7.44 (d, *J* = 8.5 Hz, 2H), 7.06 (s, 1H), 6.53 (dd, *J* = 2.4, 1.3 Hz, 1H), 5.54 (d, *J* = 4.7 Hz, 1H, O*H*), 4.88-4.83 (m, 1H), 3.97 (s, 3H, CH_3), 3.27-3.24 (m, 2H). ^{13}C NMR (75 MHz, DMSO-d$_6$) δ 150.3 ($C_{IV,Ar}$), 143.0 ($C_{IV,Ar}$), 142.5 ($C_{IV,Ar}$), 140.7 (CH_{Ar}), 139.6 (q, $^2J_{CF}$ = 37 Hz, $C_{IV,Ar}$), 138.7 ($C_{IV,Ar}$), 136.7 ($C_{IV,Ar}$), 133.8 (CH_{Ar}), 132.3 (CH_{Ar}), 127.8 ($C_{IV,Ar}$), 127.5

(CH_{Ar}), 126.7 (2xCH_{Ar}), 124.0 (CH_{Ar}), 121.4 (q, $^{1}J_{CF}$ = 266 Hz, CF_3), 118.1 (2xCH_{Ar}), 107.7 (CH_{Ar}), 105.1 (q, $^{3}J_{CF}$ = 2 Hz, CH_{Ar}), 71.9 (CH), 41.2 (CH_2), 38.4 (CH_3). HRMS (ESI+) m/z Calc. for $C_{22}H_{18}F_3N_5O_3$ $[M+H]^+$ 458.1435, found 458.1435.

1-(4-(1*H*-Pyrazol-1-yl)phenyl)-2-(4-(1-methyl-1*H*-pyrazol-4-yl)-2-nitrophenyl)ethanol (10e). The crude product was prepared according to procedure C starting from **9c** (130 mg, 0.33 mmol) and 1-methylpyrazole-4-boronic acid pinacol ester (139 mg, 0.35 mmol). After purification by column chromatography on silica gel (Petroleum ether/EtOAc 5:5 to 2:8), the pure product **10e** (98 mg, 0.25 mmol, yield *76%*) was obtained as a white solid. m.p: 166 °C. ^{1}H NMR (300 MHz, DMSO-d_6) δ 8.46 (d, J = 2.4 Hz, 1H), 8.27 (s, 1H), 8.04 (d, J = 1.6 Hz, 1H), 7.97 (s, 1H), 7,79-7,76 (m, 3H), 7.72 (d, J = 1.3 Hz, 1H), 7.41 (d, J = 8.5 Hz, 2H), 7.40 (d, J = 7.9 Hz, 1H), 6.53 (dd, J = 2.4, 1.3 Hz, 1H), 5.48 (d, J = 4.7 Hz, 1H, O*H*), 4,84-4,78 (m, 1H), 3.87 (s, 3H, CH_3), 3.17 (d, J = 6.4 Hz, 2H). ^{13}C NMR (75 MHz, DMSO-d_6) δ 150.6 ($C_{IV,Ar}$), 143.1 ($C_{IV,Ar}$), 140.7 (CH_{Ar}), 138.6 ($C_{IV,Ar}$), 136.4 (CH_{Ar}), 133.7 ($C_{IV,Ar}$), 132.2 ($C_{IV,Ar}$), 129.9 (CH_{Ar}), 128.5 (CH_{Ar}), 128.4 (CH_{Ar}), 127.5 (CH_{Ar}), 126.7 (2xCH_{Ar}), 119.8 ($C_{IV,Ar}$), 119.6 (CH_{Ar}), 118.0 (2xCH_{Ar}), 107.6 (CH_{Ar}), 72.1 (CH), 41.3 (CH_2), 38.7 (CH_3). HRMS (ESI+) m/z Calc. for $C_{21}H_{19}N_5O_3$ $[M+H]^+$ 390.1561, found 390.1559.

1-(4-(1*H*-Pyrazol-1-yl)phenyl)-2-(4-(3,5-dimethylisoxazol-4-yl)-2-nitrophenyl)ethanol (10f). The crude product was prepared according to procedure C starting from **9c** (100 mg, 0.26 mmol) and 3,5-dimethylisoxazole-4-boronic acid pinacol ester (115 mg, 0.51 mmol). After purification by column chromatography on silica gel (Petroleum ether/EtOAc 5:5), the pure product **10f** (100 mg, 0.24 mmol, yield *95%*) was obtained as a white solid. m.p: 130 °C. ^{1}H NMR (300 MHz, DMSO-d_6) δ 8.46 (d, J = 2.4 Hz, 1H), 7.89 (d, J = 1.6 Hz, 1H), 7.80 (d, J = 8.5 Hz, 2H), 7.73 (d, J = 1.4 Hz, 1H), 7.65 (dd, J = 7.8, 1.6 Hz, 1H), 7.57 (d, J = 7.8 Hz, 1H), 7.44 (d, J = 8.5 Hz, 2H),

6.53 (dd, *J* = 2.4, 1.4 Hz, 1H), 5.51 (d, *J* = 4.7 Hz, 1H, O*H*), 4,87-4,81 (m, 1H), 3.23-3.20 (m, 2H), 2.43 (s, 3H), 2.25 (s, 3H). ^{13}C NMR (75 MHz, DMSO-d_6) δ 166.0 ($C_{IV,Ar}$), 158.0 ($C_{IV,Ar}$), 150.4 ($C_{IV,Ar}$), 143.2 ($C_{IV,Ar}$), 140.7 (CH_{Ar}), 138.6 ($C_{IV,Ar}$), 133.7 (CH_{Ar}), 132.6 ($C_{IV,Ar}$), 132.1 ($C_{IV,Ar}$), 129.3 (CH_{Ar}), 127.5 (CH_{Ar}), 126.6 (2xCH_{Ar}), 123.8 (CH_{Ar}), 118.0 (2xCH_{Ar}), 114.1 ($C_{IV,Ar}$), 107.6 (CH_{Ar}), 71.9 (CH), 41.3 (CH_2), 11.3 (CH_3), 10.3 (CH_3). HRMS (ESI+) m/z Calc. for $C_{22}H_{20}N_4O_4$ $[M+H]^+$ 405.1557, found 405.1555.

1-(4-(1*H*-1,2,4-Triazol-1-yl)phenyl)-2-(4-(1-methyl-3-(trifluoromethyl)-1*H*-pyrazol-5-yl)-2-nitrophenyl)ethanol (10g). The crude product was prepared according to procedure C starting from **9f** (90 mg, 0.23 mmol) and (1-methyl-3-trifluoromethyl-1*H*-pyrazol-5-yl)boronic acid (90 mg, 0.46 mmol). After purification by column chromatography on silica gel (EtOAc), the pure product **10g** (86 mg, 0.19 mmol, yield *82%*) was obtained as a white solid. m.p: 116 °C. ^{1}H NMR (400 MHz, DMSO-d_6) δ 9.28 (s, 1H), 8.23 (s, 1H), 8.14 (d, *J* = 1.8 Hz, 1H), 7.88 (dd, *J* = 8.1, 1.8 Hz, 1H), 7.84 (d, *J* = 8.6 Hz, 2H), 7.66 (d, *J* = 8.1 Hz, 1H), 7.52 (d, *J* = 8.6 Hz, 2H), 7.07 (s, 1H), 5.62 (d, *J* = 4.7 Hz, 1H, O*H*), 4.90-4.86 (m, 1H), 3.97 (s, 3H), 3.30-3.21 (m, 2H). ^{13}C NMR (100 MHz, DMSO-d_6) δ 152.3 (CH_{Ar}), 150.3 ($C_{IV,Ar}$), 144.8 (CH_{Ar}), 142.5 ($C_{IV,Ar}$), 142.2 ($C_{IV,Ar}$), 139.6 (q, $^2J_{CF}$ = 37 Hz, $C_{IV,Ar}$), 135.7 ($C_{IV,Ar}$), 133.9 ($C_{IV,Ar}$), 133.8 (CH_{Ar}), 132.3 (CH_{Ar}), 127.9 ($C_{IV,Ar}$), 126.9 (2xCH_{Ar}), 124.1 (CH_{Ar}), 121.4 (q, $^1J_{CF}$ = 266 Hz, CF_3), 120.1 (2xCH_{Ar}), 105.2 (q, $^3J_{CF}$ = 2 Hz, CH_{Ar}), 71.9 (CH), 41.2 (CH_2), 38.5 (CH_3). HRMS (ESI+) m/z Calc. for $C_{21}H_{17}F_3N_6O_3$ $[M+H]^+$ 459.1387, found 459.1385.

1-(4-(1*H*-1,2,4-Triazol-1-yl)phenyl)-2-(4-(1-methyl-1*H*-pyrazol-4-yl)-2-nitrophenyl)ethanol (10h). The crude product was prepared according to procedure C starting from **9f** (90 mg, 0.23 mmol) and 1-methylpyrazole-4-boronic acid pinacol ester (96 mg, 0.46 mmol). After purification by column chromatography on silica gel (100% EtOAc to EtOAc/MeOH (98:2)), the pure

product **10h** (86 mg, 0.22 mmol, yield *96%*) was obtained as a yellow solid. m.p: 189 °C. ^{1}H NMR (300 MHz, DMSO-d_6) δ 9.26 (s, 1H), 8.28 (s, 1H), 8.22 (s, 1H), 8.05 (s, 1H), 7.97 (s, 1H), 7.80 (d, J = 8.2 Hz, 2H), 7.78 (d, J = 8.0 Hz, 1H), 7.47 (d, J = 8.2 Hz, 2H), 7.40 (d, J = 8.0 Hz, 1H), 5.54 (d, J = 4.6 Hz, 1H, O*H*), 4.87-4.81 (m, 1H), 3.87 (s, 3H), 3.17 (d, J = 6,1 Hz, 2H). ^{13}C NMR (75 MHz, DMSO-d_6) δ 152.2 (CH_{Ar}), 150.6 ($C_{IV,Ar}$), 144.9 (CH_{Ar}), 142.1 ($C_{IV,Ar}$), 136.4 (CH_{Ar}), 135.6 ($C_{IV,Ar}$), 133.7 ($C_{IV,Ar}$), 132.3 ($C_{IV,Ar}$), 129.8 (CH_{Ar}), 128.5 (CH_{Ar}), 128.5 (CH_{Ar}), 126.9 (2xCH_{Ar}), 119.8 ($C_{IV,Ar}$), 119.6 (CH_{Ar}), 119.0 (2xCH_{Ar}), 72.0 (CH), 41.2 (CH_2), 39.2 (CH_3). HRMS (ESI+) m/z Calc. for $C_{20}H_{18}N_6O_3$ $[M+H]^+$ 391.1513, found 391.1513.

1-(4-(1*H*-1,2,4-Triazol-1-yl)phenyl)-2-(4-(3,5-dimethylisoxazol-4-yl)-2-nitrophenyl)ethanol (10i). The crude product was prepared according to procedure C starting from **9f** (90 mg, 0.23 mmol) and 3,5-dimethylisoxazole-4-boronic acid pinacol ester (103 mg, 0.46 mmol). After purification by column chromatography on silica gel (100% EtOAc), the pure product **10i** (50 mg, 0.12 mmol, yield *54%*) was obtained as a yellow solid. m.p: 153 °C. ^{1}H NMR (300 MHz, DMSO-d_6) δ 9.26 (s, 1H), 8.22 (s, 1H), 7.90 (d, J = 1.5 Hz, 1H), 7.82 (d, J = 8.5 Hz, 2H), 7.66 (dd, J = 7.9, 1.5 Hz, 1H), 7.59 (d, J = 7.9 Hz, 1H), 7.51 (d, J = 8.5 Hz, 2H), 5.57 (d, J = 4.7 Hz, 1H, O*H*), 4.90-4.85 (m, 1H), 3.26-3.16 (m, 2H), 2.43 (s, 3H), 2.25 (s, 3H). ^{13}C NMR (75 MHz, DMSO-d_6) δ 166.0 ($C_{IV,Ar}$), 158.0 ($C_{IV,Ar}$), 152.3 (CH_{Ar}), 150.4 ($C_{IV,Ar}$), 144.9 (CH_{Ar}), 142.1 ($C_{IV,Ar}$), 135.6 ($C_{IV,Ar}$), 133.7 (CH_{Ar}), 132.6 ($C_{IV,Ar}$), 132.0 ($C_{IV,Ar}$), 129.4 (CH_{Ar}), 126.9 (2xCH_{Ar}), 123.9 (CH_{Ar}), 119.1 (2xCH_{Ar}), 114.1 ($C_{IV,Ar}$), 71.9 (CH), 41.2 (CH_2), 11.3 (CH_3), 10.3 (CH_3). HRMS (ESI+) m/z Calc. for $C_{21}H_{19}N_5O_4$ $[M+H]^+$ 406.1510, found 406.1506.

1-(4-(1*H*-1,2,4-Triazol-1-yl)phenyl)-2-(2-nitro-4-(thiazol-5-yl)phenyl)ethanol (10j). The crude product was prepared according to procedure C starting from **9f** (108 mg, 0.28 mmol) and thiazol-5-ylboronic acid pinacol ester (133 mg, 0.55 mmol). After purification by column

chromatography on silica gel (100% EtOAc to EtOAc/MeOH (98:2)), the pure product **10j** (95 mg, 0.24 mmol, yield *88%*) was obtained as a white solid. m.p: 182 °C. ^{1}H NMR (300 MHz, DMSO-d_6) δ 9.26 (s, 1H), 9.16 (s, 1H), 8.47 (s, 1H), 8.22 (s, 1H), 8.19 (s, 1H), 7.92 (d, J = 7.9 Hz, 1H), 7.82 (d, J = 8.0 Hz, 2H), 7.52 (d, J = 7.9 Hz, 1H), 7.49 (d, J = 8.0 Hz, 2H), 5.58 (d, J = 4,1 Hz, 1H, O*H*), 4.88-4.84 (m, 1H), 3.29-3.23 (m, 2H). ^{13}C NMR (75 MHz, DMSO-d_6) δ 154.6 (CH_{Ar}), 152.3 (CH_{Ar}), 150.6 ($C_{IV,Ar}$), 144.7 (CH_{Ar}), 142.1 ($C_{IV,Ar}$), 140.8 ($C_{IV,Ar}$), 136.2 (CH_{Ar}), 135.6 ($C_{IV,Ar}$), 134.2 (CH_{Ar}), 132.5 ($C_{IV,Ar}$), 130.3 ($C_{IV,Ar}$), 130.1 (CH_{Ar}), 126.9 (2xCH_{Ar}), 121.4 (CH_{Ar}), 119.1 (2xCH_{Ar}), 71.9 (CH), 41.2 (CH_2). HRMS (ESI+) m/z Calc. for $C_{19}H_{15}N_5O_3S$ $[M+H]^+$ 394.0968, found 394.0967.

Synthesis of Mosher esters 11a and 11b (Figure A, Supporting information).

Dimethylaminopyridine (DMAP) (0.5 mg, 0.0044 mmol) was added to a mixture of **10h'** or **10h''** (17.2 mg, 0.044 mmol), *(R)*-methoxyphenylacetic acid (MPA) (7.0 mg, 0.044 mmol) and *N*,*N*-dicyclohexylcarbodiimide (DCC) (9.0 mg, 0.044 mmol) in anhydrous CH_2Cl_2 (3 mL) under Ar stream. The reaction mixture was stirred at 25 °C for 12 h, cooled to 0 °C and filtered. The filtrate was evaporated and purified by column chromatography on silica gel (100% EtOAc) to furnish Mosher esters **11a** and **11b**.

Mosher ester 11a: Yield 65%. ^{1}H NMR (400 MHz, DMSO-d_6) δ 9.27 (s, 1H), 8.34 (s, 1H), 8.23 (s, 1H), 8.14 (d, J = 1.8 Hz, 1H), 8.02 (s, 1H), 7.81 (dd, J = 8.0, 1.8, 1H), 7.71 (d, J = 8.6 Hz, 2H), 7.44 (d, J = 8.1 Hz, 1H), 7.35-7.30 (m, 5H), 7.18 (d, J = 8.6 Hz, 2H), 6.06 (t, J = 7.5 Hz, 1H), 4.85 (s, 1H), 3.88 (s, 3H), 3.19 (s, 3H), 1.06 (t, J = 6.9 Hz, 2H).

Mosher ester 11b: Yield 73%. ^{1}H NMR (400 MHz, DMSO-d_6) δ 9.32 (s, 1H), 8.31 (s, 1H), 8.26 (s, 1H), 8.05 (d, J = 1.8 Hz, 1H), 7.99 (s, 1H), 7.87 (d, J = 8.6 Hz, 2H), 7.55-7.52 (m, 3H), 7.31-

7.25 (m, 5H), 7.11 (d, *J* = 8.1 Hz, 1H), 6.06-6.03 (m, 1H), 4.92 (s, 1H), 3.90 (s, 3H), 3.19 (s, 3H), 1.06 (t, *J* = 7.0 Hz, 2H).

Enantioseparation by HPLC

Enantioselective HPLC analyses were performed using stainless-steel Chiralpak IG (250 mm × 4.6 mm i.d.) and Chiralpak IG-3 (250 mm × 250 mm × 10 mm i.d.) (Daicel, Chemical Industries, Tokyo, Japan) columns. HPLC-grade solvents were used as supplied by Aldrich (Milan, Italy). The HPLC apparatus consisted of a PerkinElmer (Norwalk, CT, USA) 200 LC pump equipped with a 542 Rheodyne (Cotati, CA, USA) injector, a 1000 μL sample loop, a HPLC Perkin-Elmer oven and a Perkin-Elmer 290 detector. The signal was acquired and processed by Clarity software (DataApex, Prague, The Czech Republic).

Circular dichroism

The CD spectra of the enantiomers isolated on a semipreparative scale, dissolved in ethanol (concentration about 0.3 mg/mL) in a quartz cell (0.1 cm path length) at 25 °C, were measured using a Jasco (Jasco, Ishikawa-cho, Hachioji City, Tokyo, Japan) model J-700 spectropolarimeter in the 400−220 nm spectral range. The spectra were average computed over three instrumental scans, and the intensities are presented in terms of terms of ellipticity values (mdeg).

Biological assays

Cells and viruses. HeLa Rh cells were grown in DMEM (Gibco) supplemented with 10% heat-inactivated fetal bovine serum (FBS, Integro), and 0.075 % $NaHCO_3$ (Gibco). Cells were grown at 37 °C in a 5% CO_2 incubator at 95-99% relative humidity. RV-A02, RV-A85, RV-A89, RV-B14, RV-B42 and RV-B70 were kindly provided by K. Andries (Janssen Pharmaceutica, Beerse, Belgium). RV-A08 and RV-A28 were kindly provided by Michaele Schmidtke

(Universitätsklinikum, Jena, Germany). All RVs were cultivated in HeLa Rh cells in the presence of 30 mM $MgCl_2$.

Cell-based antiviral assay. The antiviral activity of the synthesized compounds was evaluated in a cell-based antiviral assay with MTS read-out ([3-(4,5-dimethylthiazol-2-yl)-5-(3-carboxymethoxyphenyl)-2-(4-sulfophenyl)-2H-tetrazolium]). In this assay, the (residual) metabolic activity of treated, infected cells was quantified, representing cell survival or reduction of virus-induced cytopathic effects (CPE), and thus the antiviral effect of a compound. Rhinovirus assays were performed in 96-well plate format, using DMEM supplemented with 2% FBS, 0.075% $NaHCO_3$ and 30 mM $MgCl_2$. Briefly, a serial dilution of the compound was added to cells grown to confluence in 96-well microtiter plates, followed by infection with a low virus inoculum. The cultures were incubated for 3 days at 35 °C until complete CPE was observed in the untreated, infected virus control condition (VC). After removal of the medium from each well, 100 µL of a 5% MTS-phenazine solution in phenol red-free MEM was added. Following incubation for 1 h, raw OD values were collected using a microtiter plate reader (Safire, Tecan). Values were converted to percentage of controls and the 50% effective concentration (EC_{50}, defined as the concentration of compound that should offer 50% protection against virus-induced CPE), was calculated from the dose-response curve using logarithmic interpolation. In addition, the assays were inspected by light microscope and the adverse effect of the compound on the cells was quantified by cell scoring, from which the CC_{50} (concentration at which 50% cytotoxic effect is observed) was calculated using logarithmic interpolation.

Time-of-drug-addition assay. HeLa Rh cells were allowed to adhere overnight in 96-well cell culture plates. The next day, 1 µM compound **10e**, *(S)*-**10e**, **10h**, *(R)*-**10h** and pleconaril **1** were added 2 hours before infection, at the time of infection or at 2, 4 or 6 hours after infection with

RV-B14. Virus-infected, untreated cells were used as controls. At 8 h post-infection, supernatant was removed and the cells were lysed using Cell-to-cDNA lysis buffer (Thermo Fisher Scientific). After an additional incubation at 75 °C for 15 min to inactivate DNases, intracellular viral RNA was quantified by qRT-PCR (iTaq™ Universal SYBR® Green One-Step Kit, Bio-Rad) using the following primers: 5'-GAAACACGGACACCCAAAGTA-3' and 5'-CGGCCCCTGAATGCGGCTAA-3' (Integrated DNA technologies) and PCR program: 10 min at 50 °C, 3 min at 95 °C and 40 cycles of 15 s at 95 °C and 1 min at 60 °C (Applied Biosystems 7500 Fast Real-Time PCR system). A dilution series of gBlocks (Integrated DNA technologies) was included as standards and RNA content was quantified as genome equivalents per sample.

Resistance selection by passaging. HeLa cells grown to confluence in a 24-well microtiter plate were infected with wild-type RV-B14 in the presence of **10e**, **10h** or **1** at a concentration of 4x, 2x or 1x their *in vitro* EC_{50}. When CPE was visible in the virus control (no compound), all the wells were scored for visible CPE. Next, the cell supernatant (diluted 1:10) was transferred to a 24-well plate with freshly seeded HeLa cells in the presence of the compound and incubated as before. After four passages, the putative resistant virus was sequenced by Sanger sequencing. Briefly, viral RNA was isolated using Nucleospin© RNA virus (Macherey-Nagel). Next, a cDNA fragment covering the VP1 coding sequence was produced using a one-step RT-PCR kit (Qiagen) and RV-B14-specific primers (FP 5'-CCTTATCCAGTGCTAAACTC-3' and RP 5'-GCCCGACCCCTTTCATCAC-3'). cDNA sequences were analyzed by Macrogen Inc.

Micronucleus tests

Cell cultures and metabolic activation mixture (S9 mix). Chinese Hamster Ovary cells (CHO-K1, ATCC) were used for the micronucleus assay. They were maintained in Mc Coy's 5A medium (Sigma) supplemented with 10% foetal calf serum, 1 mM glutamine and penicilline-

streptomycine (100 U/mL-10 µg/mL) and incubated during 24 hours at 37 °C in humidified atmosphere containing 5% CO_2. The liver homogenate used for metabolic activation (S9) was prepared from male Sprague-Dawley rats treated with Aroclor 1254 (500 mg/kg body weight). The S9 mix used for the test was a mixture of S9 and a solution of NADPH generating factors (Mix).The final composition of the S9 mix included 1% S9, 0.5 mM G6P and 0.4 mM NADP.

Micronucleus assay on CHO-K1 cells. The capacities of test materials to induce micronuclei were assessed according to the protocol described by Kirsch-Volders.[45] All the assays were conducted in duplicate. The CHO-K1 cells, suspended in Mac Coys'5A medium, were transferred into Labteck wells at a concentration of 100,000 cells/ml, and incubated for 24 hours at 37 °C in CO_2 (5%). When the test was performed without metabolic activation, the test substances were added to cell cultures at concentrations previously defined. A negative control containing culture medium, a solvent control containing 1% DMSO and a positive control containing 0.6 µg/ml of mitomycin C were added. When the assay was performed in the presence of metabolic activation, S9 mix metabolizing mixture was added to cell cultures at a concentration of 10%. Then the test substances were added to the cell cultures at concentrations previously defined. A negative control containing culture medium, a solvent control containing 1% DMSO and a positive control containing 5 µg/mL of benzo-[α]-pyrene were added. After 3 hours of incubation at 37 °C in CO_2 (5%), the culture medium was removed, the cells were rinsed with phosphate buffered saline (PBS), and then returned to culture in McCoy's 5A medium containing 3 µg/ml of cytochalasin B. After a 21-hour incubation period at 37 °C, cells were rinsed with phosphate buffered saline (PBS), fixed with methanol and stained with 10% Giemsa for 20 minutes.

Analysis of results. Cells were examined under a microscope at x1000 magnification. The antiproliferative activity of test substances was assessed by counting the number of binucleated cells relative to the number of mononucleated cells on a total of 500 cells for each dose (250 cells counted per well). The proliferation index (Cytokinesis Blocked Proliferative Index CBPI) was calculated using the following formula:

$$CBPI = \frac{2 * BI + MONO}{500}$$

BI : number of binucleated cells; *MONO* : number of mononucleated cells

The cytostasis index (CI%), *i.e.* the percentage of cell replication inhibition, was calculated using the following formula: CI% : 100- {100x($CBPI_{test\ material}$-1)/($CBPI_{solvent\ control}$-1).

After this step, only the doses inducing a decrease of less than 55 ± 5% of CI% as compared to the negative control were taken into account to count micronuclei. The rates of micronuclei were evaluated for the presence of independent nuclear core entities in 1000 binucleated cells per well, which corresponds to 2000 cells examined by test substance dose.

Micronuclei were identified as small nuclei well differentiated from the cell nucleus, stained in the same manner and having a diameter less than one third of that of the cell nucleus. Micronuclei rates obtained for different doses of test substances were compared to the negative control by a x2 test. The assay was considered positive if:

a dose-response relationship was obtained between the rate of micronuclei and the doses tested,

at least one of these doses induced a statistically significant increase ($P < 0.05$) in the number of micronucleated cells as compared to the negative control.

Modelling and docking analysis

All molecular modelling studies were performed on a MacPro dual 2.66 GHz Xeon running Ubuntu 14LTS. The RV capsid structures were downloaded from PDB [http://www.rcsb.org/.]: 4PDW;[39] 1NCQ;[47] 3VDD.[32] Hydrogen atoms were added to the protein, using Maestro[48] protein preparation wizard[49] and minimized, keeping all the heavy atoms fixed until an rmsd gradient of 0.05 kcal.mol^{-1}.Å^{-1} was reached. Ligand structures were built with Maestro and minimized using the MMFF94x force field until an rmsd gradient of 0.05 kcal.mol^{-1}.Å^{-1} was reached. The docking simulations were carried out by PLANTS.[50] The homology models for studied isotypes were built by Prime.[51]The sequences of the VP1 proteins were available at the Uniprot database [www.uniprot.org]: RV-B70 Q7T5Z4; RV-B42 Q7T622_9ENTO; RV-A2 Q7T662_HRV2; RV-A8 Q7T656_9ENTO; RV-A85 Q7T5X9_9ENTO; RV-A89 Q7T5X5_HRV89; Hr_A28 Q7T636_9ENTO Uniprot code respectively. The high similarity among the references and the built models enabled us to avoid any further model optimizations. The images depicted in the manuscript were generated by Pymol.[52]

ASSOCIATED CONTENT

Supporting Information. Molecular formula strings of compounds **6a-6d**, **9a-9f**, and **10a-10j**, enantioseparation and characterization of **10e** and **10h** by Mosher's protocol, micronucleus assays on CHO-K1 cells, modelling studies and CD, NMR, HRMS spectra. This material is available free of charge *via* the Internet at http://pubs.acs.org.

AUTHOR INFORMATION

Corresponding Author

* Email: patrice.vanelle@univ-amu.fr.

Author Contributions

# L.D.C and E.S. contributed equally.

Notes

The authors declare no competing financial interest.

ACKNOWLEDGEMENT

This work was supported by the Centre National de la Recherche Scientifique and Aix-Marseille Université. We thank Dr Omar Khoumeri for valuable discussions.

ABBREVIATIONS

AC, absolute configuration; AOM, Acute Otitis Media; CC_{50}, 50% cytotoxic concentration; CD, circular dichroism; CDHR-3, cadherin related family member 3; COPD, chronic obstructive pulmonary disease; CPE, cytopathic effect; EC_{50}, 50% effective concentration; HTS, High Throughput Screening; ICAM-1, intercellular adhesion molecule 1; *(rac)*, racemic; RV, rhinovirus; SI, selectivity index; TLC, thin layer chromatography; LDL, low density lipoprotein; SAR, Structure-Activity Relationship; SET, Single-Electron Transfer; VP, viral capsid protein; VC, virus control.

REFERENCES

(1) Jacobs, S. E.; Lamson, D. M.; St George, K.; Walsh, T. J. Human Rhinoviruses. *Clin. Microbio. Rev.* **2013**, *26*, 135-162.

(2) Van Benten, I.; Koopman, L.; Niesters, B.; Hop, W.; Van Middelkoop, B.; De Waal, L.; Van Drunen, K.; Osterhaus, A.; Neijens, H.; Fokkens, W. Predominance of rhinovirus in the nose of symptomatic and asymptomatic infants. *Pediatr. Allergy Immunol.* **2003**, *14*, 363-370.

(3) Chonmaitree, T.; Heikkinen, T. Viruses and acute otitis media. *Pediatr. Infect. Dis. J.* **2000**, *19*, 1005-1007.

(4) Chantzi, F. M.; Papadopoulos, N. G.; Bairamis, T.; Tsiakou, M.; Bournousouzis, N.; Constantopoulos, A. G.; Liapi, G.; Xatzipsalti, M.; Kafetzis, D. A. Human rhinoviruses in otitis media with effusion. *Pediatr. Allergy Immunol.* **2006**, *17*, 514-518.

(5) Seppälä, E.; Sillanpää, S.; Nurminen, N.; Huhtala, H.; Toppari, J.; Ilonen, J.; Veijola, R.; Knip, M.; Sipilä, M.; Laranne, J.; Oikarinen, S.; Hyöty, H. Human enterovirus and rhinovirus infections are associated with otitis media in a prospective birth cohort study. *J. Clin. Virol.* **2016**, *85*, 1-6.

(6) Winther, B. Rhinovirus infections in the upper airway. *Proc. Am. Thorac.* Soc. **2011**, *8*, 79-89.

(7) Pitkäranta, A.; Starck, M.; Savolainen, S.; Pöyry, T.; Suomalainen, I.; Hyypiä, T.; Carpen, O.; Vaheri, A. Rhinovirus RNA in the maxillary sinus epithelium of adults patients with acute sinusitis. *Clin. Infect. Dis.* **2001**, *33*, 909-911.

(8) Kim, H. C.; Choi, S. H.; Huh, J. W.; Sung, H.; Hong, S. B.; Lim, C. M.; Koh, Y. Different pattern of viral infections and clinical outcomes in patient with acute exacerbation of chronic

obstructive pulmonary disease and chronic obstructive pulmonary disease with pneumonia. *J. Med. Virol.* **2016**, *88*, 2092-2099.

(9) Peltola, V.; Waris, M.; Österback, R.; Susi, P.; Hyypiä, T.; Ruuskanen, O. Clinical effects of rhinovirus infections. *J. Clin. Virol.* **2008**, *43*, 411-414.

(10) Hershenson, M. B. Rhinovirus-induced exacerbations of asthma and COPD. *Scientifica* **2013**, *2013*, 1-12.

(11) Friedlander, S. L.; Busse, W. W. The role of rhinovirus in asthma exacerbations. *J. Allergy Cil. Immunol.* **2005**, *116*, 267-273.

(12) Gern, J. E. How rhinovirus infections cause exacerbations of asthma. *Clin. Exp. Allergy* **2015**, *45*, 32-42.

(13) Kraft, C. S.; Jacob, J. T.; Sears, M. H.; Burd, E. M.; Caliendo, A. M.; Lyon, G. M. Severity of human rhinovirus infection in immunocompromised adults is similar to that of 2009 H1N1 influenza. *J. Clin. Microbiol.* **2012**, *50*, 1061-1063.

(14) Mallia, P.; Message, S. D.; Gielen, V.; Contoli, M.; Gray, K.; Kebadze, T.; Aniscenko, J.; Laza-Stanca, V.; Edwards, M. R.; Slater, L.; Papi, A.; Stanciu, L. A.; Kon, O. M.; Johnson, M.; Johnston, S. L. Experimental rhinovirus infection as a human model of chronic obstructive pulmonary disease exacerbation. *Am. J. Respir. Crit. Care. Med.* **2011**, *183*, 734-742.

(15) Wedzicha, J. A. Role of viruses in exacerbations of chronic obstructive pulmonary disease. *Proc. Am. Thorac. Soc.* **2004**, *1*, 115-120.

(16) Goffard, A.; Lambert, V.; Salleron, J.; Herwegh, S.; Engelmann, I.; Pinal, C.; Pin, I.; Perrez, T.; Prévotat, A.; Dewilde, A.; Delhaes, L. Virus and cystic fibrosis: rhinoviruses are associated with exacerbations in adult patients. *J. Clin. Virol*. **2014**, *60*, 147-153.

(17) De Almeida, M. B.; Zerbinati, R. M. ; Tateno, A. F.; Oliveira, C. M.; Romao, R. M.; Rodrigues, J. C.; Pannuti, C. S.; Da Silva Filho, L. F. V. Rhinovirus C and respiratory exacerbations in children with cystic fibrosis. *Emerg. Infect. Dis*. **2010**, *16*, 996-999.

(18) Royston, L.; Tapparel, C. Rhinoviruses and respiratory enteroviruses: not as simple as ABC. *Viruses* **2016**, *8*, 16.

(19) Palmenberg, A. C.; Spiro, D.; Kuzmickas, R.; Wang, S.; Djikeng, A.; Rathe, J. A.; Fraser-Liggett, C. M.; Liggett, S. B. Sequencing and analyses of all known human rhinovirus genomes reveal structure and evolution. *Science* **2009**, *324*, 55.

(20) Oliveira, M. A.; Zhao, R.; Lee, W-M; Kremer, M. J.; Minor, I.; Rueckert, R. R.; Diana, G. D.; Pevear, D. C.; Dutko, F. J.; McKinlay, M. A.; Rossmann, M. G. The structure of human rhinovirus 16. *Structure* **1993**, *1*, 51-68.

(21) Hewat, E. A.; Blaas, D. Cryoelectron microscopy analysis of the structural changes associated with human rhinovirus type 14 uncoating. *J. Virol.* **2004**, *78*, 2935-2942.

(22) Garriga, D.; Pickl-Herk, A.; Luque, D.; Wruss, J.; Castón, J. R.; Blaas, D.; Verdaguer N. Insights into minor group rhinovirus uncoating: the X-ray structure of the HRV2 empty capsid. *PLoS Pathogens* **2012**, *8*, e1002473.

(23) Verdaguer, N.; Fita, I.; Reithmayer, M.; Moser, R.; Blaas, D. X-ray structure of a minor group human rhinovirus bound to a fragment of its cellular receptor protein. *Nat. Struct. Mol. Biol.* **2004**, *11*, 429-434.

(24) Greve, J. M.; Davis, G.; Meyer, A. M.; Forte, C. P.; Yost, S. C.; Marlor, C. W.; Kamarck, M. E.; McClelland, A. The major human rhinovirus receptor is ICAM-1. *Cell* **1989**, *56*, 839-847.

(25) Hofer, F.; Gruenberger, M.; Kowalski, H.; Machat, H.; Huettinger, M.; Kuechler, E.; Blaas, D. Members of the low density lipoprotein receptor family mediate cell entry of a minor-group common cold virus. *Proc. Natl. Acad. Sci. USA* **1994**, *91***,** 1839-1842.

(26) Bochkov, Y. A.; Watters, K.; Ashraf, S.; Griggs, T. F.; Devries, M. K.; Jackson, D. J.; Palmenberg, A. C.; Gern, J. E. Cadherin-related family member 3, a childhood asthma susceptibility gene product, mediates rhinovirus C binding and replication. *Proc. Natl. Acad. Sci. USA* **2015**, *112*, 5485-5490.

(27) Palmenberg, A. C. Rhinovius C, asthma, and cell surface expression of virus receptor CDHR3. *J. Virol.* **2017**, *91*, e00072-17.

(28) Katpally, U.; Smith, T. J. Pocket factors are unlikely to play a major role in the life cycle of human rhinovirus. *J. Virol.* **2007**, *81*, 6307-6315.

(29) Patick, A. K.; Binford, S. L.; Brothers, M. A.; Jackson, R. L.; Ford, C. E.; Diem, M. D.; Maldonado, F.; Dragovich, P. S.; Zhou, R.; Prins, T. J.; Fuhrman, S. A.; Meador, J. W.; Zalman,

L. S.; Matthews, D. A.; Worland, S. T. *In vitro* antiviral activity of AG7088, a potent inhibitor of human rhinovirus 3C protease, *Antimicrob. Agents Chemother.* **1999**, *43*, 2444-2450.

(30) Lacroix, C.; George, S.; Leyssen, P.; Hilgenfeld, R.; Neyts, J. The enterovirus 3C protease inhibitor SG85 efficiently blocks rhinovirus replication and is not cross-resistant with rupintrivir. *Antimicrob. Agents Chemother.* **2015**, *59*, 5814-5818.

(31) De Palma, A. M.; Vliegen, I.; De Clercq, E.; Neyts, J. Selective inhibitors of picornavirus replication. *Med. Res. Rev.* **2008**, *6*, 823-884.

(32) Feil, S. C.; Hamilton, S.; Krippner, G. Y.; Lin, B.; Luttick, A.; McConnell, D. B.; Nearn, R.; Parker, M. W.; Ryan, J.; Stanislawski, P. C.; Tucker, S. P.; Watson, K. G.; Morton, C. J. An orally available 3-ethoxybenzisoxazole capsid binder with clinical activity against human rhinovirus. *ACS Med. Chem. Lett.* **2012**, *3*, 303-307.

(33) Makarov, V. A.; Braun, H.; Richter, M.; Riabova, O. B.; Kirchmair, J.; Kazakova, E. S.; Seidel, N.; Wutzler, P.; Schmidtke, M. Pyrazolopyrimidines: potent inhibitors targeting the capsid of rhino- and enteroviruses. *ChemMedChem* **2015**, *10*, 1629-1634.

(34) Kim, J.; Jung, Y. K.; Kim, C., Shin, J. S.; Scheers, E.; Lee, J-Y; Han, S. B.; Lee, C-K; Neyts, J.; Ha, J-D; Jung, Y-S. A novel series of highly potent small molecule inhibitors of rhinovirus replication. *J. Med. Chem.* **2017**, ***13,* 5472-5492.**

(35) Fois, B.; Bianco, G.; Sonar, V. P.; Distinto, S.; Maccioni, E.; Meleddu, R.; Melis, C.; Marras, L.; Pompei, R.; Floris, C.; Caboni, P.; Cottiglia, F. Phenylpropenoids from *Bupleurum*

fruticosum as anti-human rhinovirus species A selective capsid binders. *J. Nat. Prod.* **2017**, *80*, 2799-2806.

(36) Diana, G. D.; Rudewicz, P.; Pevear, D. C.; Nitz, T. J.; Aldous, S. C.; Aldous, D. J.; Robinson, D. T.; Draper, T.; Dutko, F. J.; Aldi, C. Picornavirus inhibitors: trifluoromethyl substitution provides a global protective effect against hepatic metabolism. *J. Med. Chem.* **1995**, *38*, 1355-1371.

(37) Cornebise, M. A.; Atherton, J.; Bist, S.; Butler, S.; Grebe, T. P.; Hentemann, M.; Huang, J.; Johnson, K. D.; Kawatkar, S. P.; McCrea, C.; Martin, L.; Mondal, M.; Rooney, M.; Thakur, K.; Tiong-Yip, C. L.; Wang, J.; Yu, Q. Discovery of AZN001: a broad-spectrum capsid-binding human rhinovirus inhibitor, Abstracts of Papers, *252nd ACS National Meeting & Exposition*, Philadelphia, PA, United States, August 21-25, **2016**.

(38) Roche, M.; Lacroix, C.; Khoumeri, O.; Franco, D.; Neyts, J.; Terme, T.; Leyssen, P.; Vanelle, P. Synthesis, biological activity and structure-activity relationship of 4,5-dimethoxybenzene derivatives inhibitor of rhinovirus 14 infection. *Eur. J. Med. Chem*. **2014**, *76*, 445-459.

(39) Lacroix, C.; Querol-Audí, J.; Roche, M.; Franco, D.; Froeyen, M.; Guerra, P.; Terme, T.; Vanelle, P.; Verdaguer, N.; Neyts, J.; Leyssen, P. A novel benzonitrile analogue inhibits rhinovirus replication. *J. Antimicrob. Chem.* **2014**, *69*, 2723-2732.

(40) Da Costa, L.; Roche, M.; Scheers, E.; Coluccia, A.; Neyts, J.; Terme, T.; Leyssen, P.; Silvestri, R.; Vanelle, P. VP1 crystal structure-guided exploration and optimization of 4,5-

dimethoxybenzene-based inhibitors of rhinovirus 14 infection. *Eur. J. Med. Chem*. **2016**, *115*, 453-462.

(41) Da Costa, L.; Scheers, E.; Coluccia, A.; Rosetti, A.; Roche, M.; Neyts, J.; Terme, T.; Cirilli, R.; Mirabelli, C.; Silvestri, R.; Vanelle, P. Heterocyclic pharmacochemistry of new rhinovirus antiviral agents: A combined computational and experimental study. *Eur. J. Med. Chem.* **2017**, *140*, 528-541.

(42) Broggi, J.; Terme, T.; Vanelle, P. Organic electron donors as powerful single-electron reducing agents in organic synthesis. *Angew. Chem. Int. Ed.* **2014**, *53*, 384-413.

(43) Lacroix, C.; Laconi, S.; Angius, F.; Coluccia, A.; Silvestri, R.; Pompei, R.; Neyts, J.; Leyssen, P. *In vitro* characterisation of pleconaril/pirodavir-like compound with potent activity against rhinoviruses. *J. Virol.* **2015**, *12*, 1-6.

(44) Rossmann, M. G. The structure of antiviral agents that inhibit uncoating when complexed with viral capsids. *Antiviral Res.* **1989**, *11*, 3-13.

(45) Kirsch-Volders, M.; Elhajouji, A.; Cundari, E.; Van, Hummelen P. The *in vitro* micronucleus test: a multi-endpoint assay to detect simultaneously mitotic delay, apoptosis, chromosome breakage, chromosome loss and non-disjunction. *Mutat Res.* **1997**, *392*, 19-30.

(46) Ledford, R. M.; Patel, N. R.; Demenczuk, T. M.; Watanyar, A.; Herbertz, T.; Collet, M.S.; Pevear, D. C. VP1 sequencing of all human rhinovirus serotypes: insights into genus phylogeny and susceptibility to antiviral capsid-binding compounds. *J. Virol.* **2004**, *78*, 3663-3674.

(47) Zhang, Y.; Simpson, A. A.; Ledford, R. M.; Bator, C. M.; Chakravarty, S.; Skochko, G. A.; Demenczuk, T. M.; Watanyar, A.; Pevear, D. C.; Rossmann, M. G. Structural and virological studies of the stages of virus replication that are affected by antirhinovirus compounds. *J. Virol.* **2004**, 78, 11061-11069.

(48) Small-Molecule Drug Discovery Suite 2015-1, Schrödinger, LLC, New York, NY, **2017**.

(49) Sastry, G. M.; Adzhigirey, M.; Day, T.; Annabhimoju, R.; Sherman, W. Protein and ligand preparation: parameters, protocols, and influence on virtual screening enrichments. *J. Comput. Aid. Mol. Des.* **2013**, *27*, 221-234.

(50) Korb, O.; Stutzle, T.; Exner, T. E. PLANTS: Application of Ant Colony Optimization to Structure-Based Drug Design. In *Ant Colony Optimization and Swarm Intelligence*; Dorigo, M.; Gambardella, L. M.; Birattari, M.; Martinoli, A.; Poli, R.; Stutzle, T., Eds.; ANTS **2006**, Lecture Notes in Computer Science, Springer, Berlin, Heidelberg, *4150*, 247-258.

(51) Jacobson, M. P.; Pincus, D. L.; Rapp, C. S.; Day, T. J. F.; Honig, B.; Shaw, D. E.; Friesner, R. A. A hierarchical approach to all-atom protein loop prediction. *Proteins: structure, function and bioinformatics.* **2004**, *55*, 351-367.

(52) PyMOL version 1.2r1; DeLanoScientificLLC: SanCarlos, CA. http://www.pymol.org/

Table of Contents Graphic

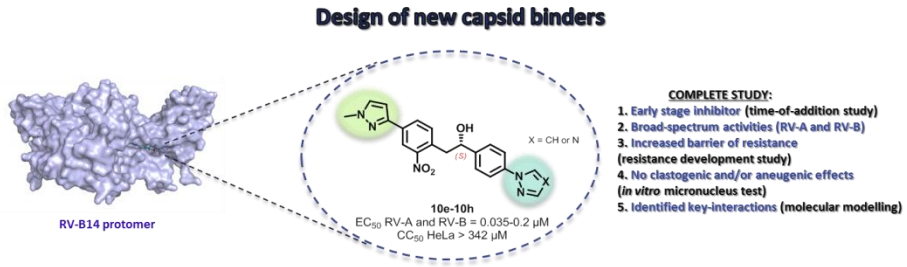

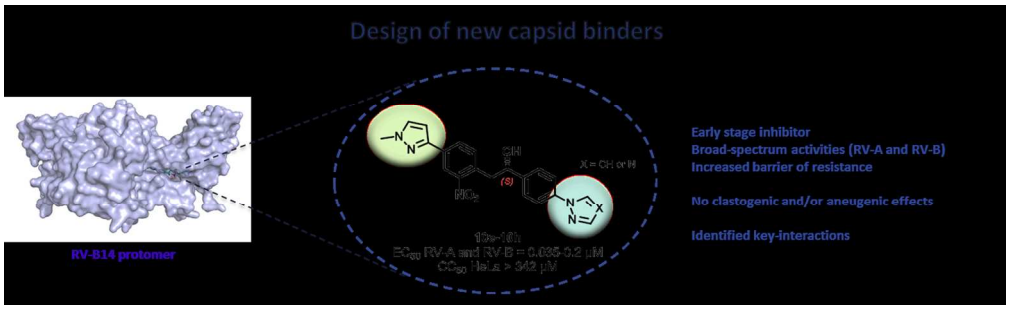

122x36mm (300 x 300 DPI)